Role of sugars in the inactivation of horseradish peroxidase induced by cold atmospheric plasma

Highlights

Cold atmospheric plasma (CAP) can reduce the activity of horseradish peroxidase (HRP)

The inactivation efficiency depends on plasma exposure time and ozone concentration

Cold atmospheric plasma affected the HRP tertiary and secondary structures

Sugars reduced the CAP efficacy with a concentration-dependent effect

Disaccharides protect more than monosaccharides the HRP activity and conformation

Role of sugars in the inactivation of horseradish peroxidase induced by cold atmospheric plasma

Jessica Laika[a], Giampiero Sacchetti[a], Annalaura Sabatucci[a], Junior Bernardo Molina-Hernandez[a], Antonella Ricci[a], Romolo Laurita[bc], Silvia Tappi[de], Alessandro Di Michele[f], Lilia Neri[a]*

[a] Department of Bioscience and Technology for Agriculture, Food and Environment, University of Teramo, Via R. Balzarini 1, 64100 Teramo, Italy.
[b] Department of Industrial Engineering, Alma Mater Studiorum-Università di Bologna, 40136 Bologna, Italy
[c] Interdepartmental Centre for Industrial Research in Health Sciences and Technologies - CIRI Health Sciences and Technologies Alma Mater Studiorum-Università di Bologna, 40136 Bologna, Italy
[d] Department of Agricultural and Food Sciences, University of Bologna, 47521 Cesena, Italy.
[e] Interdepartmental Centre for Agri-Food Industrial Research, University of Bologna, via Quinto Bucci 336, 47521 Cesena (FC), Italy.
[f] Department of Physics and Geology, University of Perugia, via Pascoli, 06123 Perugia, Italy.

* Correspondence: lneri@unite.it

Abstract

This study investigated the effect of different CAP exposures on the activity of horseradish peroxidase (HRP) in phosphate buffer and in model systems with different concentrations of monosaccharides (glucose, fructose) and disaccharides (sucrose, trehalose) to evaluate the potential role of sugars in enzyme inactivation. Spectroscopic analyses (fluorescence, circular dichroism, UV-Vis absorption) were conducted to highlight structural modifications possibly responsible for HRP inactivation. In phosphate buffer, the inactivation of HRP by CAP resulted dependent on both the treatment time (up to 70% after 30 min) and ozone concentration in the chamber. HRP residual activity was fitted with a very good approximation by the Weibull model. Sugars reduced the CAP efficacy, and this effect was concentration-dependent and much higher for disaccharides than monosaccharides. UV and fluorescence spectra showed that sugars differently preserved HRP tertiary structure, hindering heme degradation and quenching of aromatic amino acids. Likewise, sugars differently affected the loss of secondary structures. These findings only partially explained the diverse protective effects of sugars on HRP. Other factors, such as the different sugars' abilities to quench plasma reactive species, reduce the system mobility, and stabilize proteins by preserving their hydration shell, were retained to play a role in the reduction of HRP inactivation. This study deepened the knowledge of the effect of CAP on peroxidase activity and demonstrated that the presence of mono and disaccharides, naturally found in fruits and vegetables and widely employed in food and beverage industries, can mitigate the inactivation and structural alterations induced by CAP on peroxidase enzymes.

Keywords: Cold plasma, horseradish peroxidase, sugars, inactivation models, UV-Vis and fluorescence spectroscopy, circular dichroism.

1. Introduction

Enzymatic inactivation is one of the most relevant challenges in fruit and vegetable processing. It is well recognized that the loss of quality parameters such as color, flavor, texture, and nutritional characteristics in raw, minimally or fully processed fruits and vegetables is due to the activity of residual endogenous enzymes (Matsui et al., 2007; Misra et al., 2016).

Over the past decades, several physical and chemical treatments have been developed to inactivate or control the activity of food endogenous enzymes. Thermal treatments are conventionally used for enzymatic inactivation, however, some heat-sensitive constituents such as vitamins, anthocyanins, polyphenols, and flavonoids can be destroyed, and a detrimental impact on products' color, flavor, and nutritional properties can occur (Y. X. Han et al., 2019). Chemical processes, including organic acids like oxalic acid (Lo'ay & Dawood, 2017), citric acid, and ascorbic acid (Surowsky et al., 2013), can lead to the reduction of enzyme activity with low pH (Tsouvaltzis & Brecht, 2017). However, they present some drawbacks linked to their cost, management, recycling of wastes and production of chemical residues potentially dangerous to human health; hence, the interest of food industries and researchers to replace these techniques and produce clean label products through the use of non-thermal processing technologies (Gui et al., 2006; Hollósy, 2002; Jang & Moon, 2011; Préstamo et al., 2001; B. Wang et al., 2017; Zhong et al., 2005).

Among these, cold atmospheric plasma (CAP) represents a great potential technology for the agriculture and food industry (X. Y. Dong & Yang, 2019; Ekezie et al., 2019; Mir et al., 2016; Pan et al., 2019). CAP consists of ultraviolet (UV) photons, ions, free electrons, and reactive species such as active nitrogen (RNS) and active oxygen (ROS) (Ekezie et al., 2019; Y. Han et al., 2019; Pankaj et al., 2013) and has been proved to be effective in residue degradation (Sarangapani et al., 2018) and microbial decontamination (Punia Bangar et al., 2022). Moreover, several studies carried out on model systems (Surowsky et al., 2013; Zhang et al., 2015) and/or in real liquid or solid food systems (Y. Han et al., 2019; Tappi et al., 2014, 2016; Y. Wang et al., 2021) have also highlighted the capability of CAP to affect endogenous food enzymes such as peroxidase, polyphenol oxidase, lysozyme, a-chymotrypsin, alkaline phosphatase, and pectin methylesterase due to the interaction of plasma reactive species with amino acids and secondary structure. However, as recently discussed by (Y. Han et al., 2019) in a recent review, the effect of CAP on food enzymes can be variable and result in the inactivation or activation of proteins, depending on several factors such as the type of protein, the plasma composition, the equipment configuration, the sample volume, and the treatment time. Moreover, food matrices are complex systems composed of several natural and/or added components that can influence the effect of CAP on enzymatic inactivation due to the interaction with plasma reactive species (Fernandes & Rodrigues, 2021) and proteins themselves by affecting their

thermodynamic and/or kinetic stability (Barbiroli et al., 2017; Timasheff, 1993). Sugars and polyols, in particular, are particularly susceptible to the action of plasma reactive species (Li et al., 2014); according to their molecular structure and concentration, sugars were shown to have different scavenging activity and capability to protect proteins from being oxidized (Surowsky et al., 2016). Moreover, sugars are well known for their protection and stabilizing effect on protein structures due to their ability to affect proteins' hydration shell density. In diluted systems, sugars are solubilized in bulk water and preferentially excluded from the protein surface (Ajito et al., 2018; Lee & Timasheff, 1981). The modifications of the protein-solvent interaction lead to the increase of the system free energy that favors the folded state of the protein (Arakawa & Timasheff, 1982), which results in less active but more stable (Sola-Penna & Meyer-Fernandes, 1994, 1998). This concept, known as preferential exclusion theory, is nowadays most widely accepted to explain the protective and stabilization mechanism (Barbiroli et al., 2017; Corezzi et al., 2021) of sugars on proteins upon thermal (Faieta et al., 2020), chemical (Sola-Penna et al., 1997; Aijito et al., 2018), and non-thermal food processes (Faieta et al., 2021).

To deepen the understanding of the impact of CAP on food enzymes and to assess, for the first time, the potential influence of sugars on their inactivation, this study aimed to investigate the effect of different monosaccharides (glucose and fructose) and disaccharides (sucrose and trehalose), naturally present in fruits and vegetables and extensively utilized by industries for the production of foods and beverages, on the inactivation of horseradish peroxidase (HRP) induced by cold atmospheric plasma. Furthermore, to gain insight into the enzyme inactivation mechanisms, besides the catalytic activity, measurements of changes in protein conformation and tryptophan fluorescence were also determined before and after CAP treatments.

HRP was chosen as the target enzyme since it is the most widely studied among peroxidases and its biochemical properties and structure are well known (Chattopadhyay & Mazumdar, 1999). Peroxidases occur naturally in nearly all plants and animals and, due to their non-specific action, show a detrimental effect on many biological systems and foods where they cause off-colors and off-flavors formation (Burnette, 1977; Pizzocaro et al., 1994; Richter Reis, 2023; Tijskens et al., 1997). Moreover, because of the high thermostability, the activity of this endogenous enzyme is conventionally used as an index of the efficiency of thermal treatments aimed at preserving fruits and vegetables upon processing and storage. Consequently, its determination allows comparison and evaluation of the effectiveness and potential application of cold atmospheric plasma for innovative and sustainable processing of heat-sensitive fruits and vegetable products.

2. Materials and methods

2.1 Materials

Potassium phosphate and glucose were obtained from Sigma (Steinheim, Germany), fructose was purchased from VWR International (Leuven, Belgium), sucrose (from Thermo Fisher Scientific (Kandel, Germany), and trehalose monohydrated from Cargill (Milan, Italy). All chemicals were of analytical grade. Horseradish peroxidase (EC 1.11.1.7) was obtained from Sigma (Steinbach, Germany).

2.2 Model systems preparation

All the model systems were prepared using 0.1 M potassium phosphate buffer (pH 6.5). Sugars and HRP were added and dissolved into the buffer solution to obtain ternary systems characterized by a final enzyme concentration of 0.5 mg ml^{-1} and the following sugar concentrations: 18.36% (w/w) (G1) and 31.03% (w/w) (G2) of glucose; 18.36% (w/w) (F1) and 31.75% (w/w) (F2) of fructose; 29.97% (w/w) (S1) and 42.96% (w/w)(S2) of sucrose; 31.05% (w/w) (T1) and 46.24% (w/w) (T2) of trehalose. These co-solute concentrations were selected to obtain systems characterized by an equal sugar molality (1.25 mol/kg) and/or equal water activity values (a_w 0.98 for and 0.95), to highlight and compare the specific effects exerted by different sugars on protein conformational and activity changes before and upon cold plasma treatments. A binary system (PBS) used as a reference sample was also produced by dissolving HRP in the buffer solution up to a final concentration of 0.5 mg ml^{-1}. All the model systems were prepared just before the CAP treatment or analysis.

2.3 Cold atmospheric plasma device and experimental set-up

All the treatments were performed by using the device "Plasma Assisted Sanification System" (PASS), developed by AlmaPlasma srl (Bologna, Italy). As described by Molina-Hernandez et al. (2022), this CAP system is composed of a surface dielectric barrier discharge plasma source (SDBD), a treatment chamber, a cooling system, and a high-voltage generator. The plasma source consists of 4 rectangular high-voltage electrodes (115 cm^2 each) and a mica dielectric layer over 2 mm thick. The ground electrode had the shape of a mesh and was in contact with the dielectric layer, whereas the plasma was formed in the holes of the mesh, producing an indirect treatment. The treatment chamber is made of poly(methyl methacrylate) (PMMA), and when the SDBD is placed on the top of the treatment chamber, a closed volume of $18.5*10^3$ cm^3 is defined. The device, operating in environmental air (relative humidity in the range 20–40%), was driven by a high-voltage generator (AlmaPULSE, AlmaPlasma srl, Bologna, Italy), allowing the application of 6 kV, with a frequency of 23 kHz, and a 10% duty cycle A sinusoidal waveform was applied to the high-voltage electrode

with a 6 kV of amplitude at 23 kHz. The temperature inside the treatment chamber was measured during the discharge time using a fiber optical temperature sensor (opSense, OTG series).

Before the CAP treatments, 950 µl of each model system were added into a 35 mm diameter six-well plate. This volume was chosen to get a layer of liquid 1 mm high in each well. Thus, the plates were located on the base of the treatment chamber and finally exposed to plasma treatments for 5, 10, 20, and 30 min. After the treatments, the samples were immediately transferred into Eppendorf tubes and kept under ice and in the dark until analyses. Each treatment was carried out in duplicate.

2.4 Water activity, pH, and viscosity

Water activity was measured at 25 °C using a dew point hygrometer AcquaLab CX 2 (Acqualab Scientific Pty Ltd., Castel Hill, NSW). Calibration with different saturated salt solutions having different Equilibrium Relative Humidity (ERH%) was performed before analysis.

The pH values were determined with a laboratory pH meter (MP220, Mettler Toledo International, Polaris Parkway, USA). All measurements were performed in triplicate.

Viscosity was measured at 20 °C using a Haake (Karlsruhe, Germany) Thermo type C falling ball viscometer. The measurements were carried out using a boron silica glass ball and a nickel-iron alloy ball with a density of 2.2 and 8.1 g cm^{-3} and k values of 0.09 and 0.09 mPa s cm^3 g^{-1} s^{-1}, respectively. The apparent dynamic viscosity (millipascal second) was measured using the following equation:

$$\eta = k(\rho_1 - \rho_2)\, t$$

k=ball constant in millipascal second cube centimeter per gram per second; ρ_1=density of the ball in gram per cube centimeter; ρ_2=density of the liquid to be measured at the measuring temperature in gram per cube centimeter; t=falling time of the ball in seconds. The falling time of the ball was determined by using a stopwatch. The density of each solution was measured at 25 °C by using a hydrostatic balance (Gibertini, Milan, Italy). The kinematic viscosity of the solutions was calculated by the viscosity-to-density ratio and expressed as centiStokes (10^{-6} m^2 s^{-1}).

2.5 Peroxidase assay

The HRP activity of the model systems was assessed before and after the CAP treatments spectrophotometrically using a microplate reader (Multi-mode Plate Reader EnSpire, Perkin Elmer). According to Keesey (1987), a 20 mM solution of 2,2′-azinobis-(-3ethylbenzothiazoline-6-sulfononic acid) diammonium salt (ABTS) (pH 6.5) was used as reaction substrate. The HRP assay was performed by adding into each well of a 96-well plate 3 µl of the sample, 135 µl of ABTS 20 mM, and finally, 65 µl of hydrogen peroxide at the concentration of 0.03% (w/w) as an oxidant to start the reaction. The HRP activity was measured at 25 °C by monitoring the increase in absorbance at 405 nm for 3 minutes. Each sample was analyzed in triplicate.

The reaction rate was computed from the slope (ΔA/min) of the initial linear portion of the plot of absorbance vs. time. The residual enzymatic activity was calculated according to the following equation:

$$R_A = \frac{A}{A_0} \times 100$$

where R_A is the residual peroxidase activity expressed in percentage; A and A_0 show the sample absorption rate after cold plasma treatment and the absorption rate of the untreated sample, respectively. One unit (U) was defined as the quantity of enzyme necessary to obtain an increase in absorbance of 1U in 1 min under the assay conditions.

2.6 UV-Vis spectral analysis

Ternary and binary systems characterized by an HRP concentration of 0.5 mg ml^{-1} were analyzed before and after the CAP treatment. 200 µl of each sample were added into an individual well of a 96-well plate and scanned within the spectral range of 230–600 nm using a microplate reader (Multi-mode Plate Reader EnSpire, Perkin Elmer, USA). The spectra of the samples were then subtracted from those of the corresponding model system without the enzyme. Thus, the Reinheitzahl parameter (Rz), i.e., the absorbance ratio between the Soret absorbance band (λ=403 nm) and the absorbance at λ=275, was calculated for each spectrum to determine changes in HRP hemin content (Pellicer & Gómez-López, 2017). Each sample was analyzed in duplicate.

2.7 Fluorescence measurements

Ternary and binary systems characterized by an HRP concentration of 0.5 mg ml^{-1} were analyzed before and after the CAP treatment. Fluorescence emission spectra of intrinsic Trp residues of peroxidase were measured using a microplate reader (Multi-mode Plate Reader EnSpire, Perkin Elmer, USA). The emission spectra were collected in duplicate in the range of 300–400 nm at an excitation wavelength of 280 nm and 400–500 nm at an excitation wavelength of 330 nm. For the analysis, no further sample preparation was required.

2.8 Circular dichroism spectroscopy

Circular dichroism (CD) measurements were carried out exclusively on PBS and sugar model systems having equal molality (G1, F1, S1, T1), before and after 30 minutes of treatment, by using a spectropolarimeter (Jasco model J-810, Oklahoma City, Oklahoma, USA). Measurements were performed using a quartz cell of 0.1 cm path length. The initial concentration of peroxidase in the samples was 11,36 µM. According to Surowsky et al. (2013), the CD spectrum was recorded in duplicate between 200 and 260 nm at a scan rate of 50 nm min^{-1}. The baseline, made with phosphate buffer solution, was also recorded. The instrument lamp was purged with nitrogen before and during

the performance of the measurements. The ellipticity data were obtained in millidegrees (mdeg). The secondary structure estimation of proteins from the CD spectra was performed by CDNN software.

2.9 Kinetic modeling

To model the kinetics of HRP inactivation due to the exposure time to CAP treatment, data were fitted by using a first-order model:

$$\ln A_t = \ln A_0 - k \cdot t \quad (1)$$

where A_t is the residual enzymatic activity at time t, A_0 is the initial enzymatic activity, and k is the reaction rate constant.

To model the kinetics of O_3 production as a function of time, data were fitted by the Peleg model (Peleg, 1988)

$$C_t = C_0 + \frac{t}{k_1 + k_2 t} \quad (2)$$

where C_t is the concentration at time t, C_0 is the initial concentration, and k_1 and k_2 are constants. The reciprocal of k_1 represents the initial O_3 production rate while the sum of C_0 and the reciprocal of k_2 represents the O_3 concentration at infinite time.

Then, time was explicated as a function of concentration as follows:

$$t = \frac{C_t k_1 - C_0 k_1}{1 - C_t k_2 + C_0 k_2} \quad (3)$$

and equation (3) was substituted in the first-order model to express the enzymatic inactivation as a function of ozone concentration.

The HRP inactivation kinetic upon CAP exposure time was also fitted by a normalized Weibull equation (De Fátima Machado et al., 1998; De Flaviis & Sacchetti, 2022):

$$C_t = C_0 + (C_\infty - C_0)[1 - e^{-\left(\frac{t}{\alpha}\right)^\beta}] \quad (4)$$

where C_∞ is the concentration at the equilibrium and β and α are the shape and scale parameters, respectively; α represents the time needed to reach the 63.2% of the inactivation (C_0–C_∞) whilst the reciprocal of β could be intended as a measurement of the initial rate of the process (Sacchetti et al., 2005).

C_∞ was constrained to 0, and t was eventually substituted with equation (3).

The goodness of fit of the models was evaluated considering the R^2, the root means square error (RMSE), and the distribution of the residuals.

2.10 Statistical analysis

All data were analyzed (ANOVA) with Statistica, TIBCO Software Inc. (2018), (data analysis software system version 13), and XLSTAT 2021 software (Data Analysis and Statistical Solution for Microsoft Excel, Addinsoft, Paris, France). Pearson's correlation coefficient (r) was used to determine significant ($p < 0.05$) correlation among variables.

Significant differences between means were determined by Fisher's LSD test ($p < 0.05$). In the figures, the mean variability of data was indicated by the standard deviation.

3. Results and discussion

3.1. Concentration of reactive oxygen and nitrogen species (rons) produced by CAP

Plasma composition was evaluated by determining the concentrations of ozone and nitrogen dioxide in the chamber at different process times. The tests were performed three times. According to other authors (Molina-Hernandez et al., 2022; Pavlovich et al., 2014), the low power conditions promoted the production and accumulation over time of ozone (Fig. 1), while nitrogen dioxide concentration was below the detection limit (<5.5 ppm), indicating operating O_3 regime. O_3 concentration data over time were thus modeled by using the Peleg equation which showed a nearly perfect fit of the experimental data (Fig. 1 insert).

3.2 Inactivation and structural changes of HRP in buffer system induced by CAP

3.2.1 HRP inactivation

The inactivation kinetics of HRP in phosphate buffer is shown in Fig. 2. It can be observed that the HRP activity decreased at the increase of the treatment time reaching after 30 minutes a residual activity of about 30%. As the temperatures recorded within the chamber were below 30 °C, the temperature was a negligible factor in the inactivation of the enzyme (Y. X. Han et al., 2019). Similarly, the pH did not contribute to the HRP inactivation since after each treatment it resulted unchanged ($p<0.01$). These results indicate that ozone and possibly other reactive species (RS) generated by its interaction with the liquid phase (Dharini et al., 2023), such as •OH and H_2O_2 were involved in the enzyme inactivation. The effectiveness of cold plasma in peroxidase inactivation was also highlighted by other authors in both model (Ke & Huang, 2013; Surowsky et al., 2013) and real food systems (Thirumdas & Annapure, 2020), however, different inactivation percentages were found depending on the composition, the type of equipment, gas and process conditions employed.

3.2.2 Data modelling

Data were fitted using a first-order model and the Weibull distribution model (Fig. 3a). The value of the inactivation rate constant (K_p) of the first-order model and the values of the scale (α) and shape

(β) parameters of the Weibull model along with the corresponding RMSE and R^2 were reported in Fig. 3a (insert). It can be observed that HRP residual activity was not satisfactorily described by the first-order model, while the Weibull model well predicted the HRP residual activity as shown respectively by the high R^2 and low RMSE values. This same result was also found by other authors (Chutia et al., 2019; Pankaj et al., 2013) and may imply that the inactivation of the enzyme is not simply related to the disruption of a single bond or structure but is dependent on different phenomena (Adams, 1991; Pankaj et al., 2013).

Then, to explicate the HRP inactivation as a function of the O_3 concentration, HRP inactivation data after different exposure times to CAP were fitted by the Weibull distribution explicating the time as a function of the O_3 concentration, as described by the Peleg model (Fig. 1). As shown (Fig. 3b) and depicted by the high R^2 and low RMSE values (Fig. 3b, insert), the proposed model strongly described the experimental data.

3.2.3 Absorption spectra

HRP structural changes induced by CAP treatments were assessed by examining its absorption spectrum before and after different CAP exposure times (Fig. 4). The UV-Vis spectra of the untreated sample showed one peak at about 275 nm, given by the absorption of HRP aromatic residues such as tryptophan (Trp) and tyrosine (Tyr) and to a small extent by the absorbance of disulfide bonds, and the Soret and Q bands respectively at 403 nm at 498 nm resulting from heme absorption (Pellicer & Gómez-López, 2017; Ravanfar & Abbaspourrad, 2021).

The UV-Vis spectra of HRP buffered systems exposed to different CAP treatments showed a decrease of the Soret band and the loss of the peak at 275 nm, and the extent of these variations was dependent on the CAP exposure time. The loss of the peak at 275 nm, particularly notable in the sample treated for 30 min, highlights possible protein aggregation (Y. X. Han et al., 2019). The Reinheitzahl parameter (Rz) was evaluated for each spectrum to determine changes in HRP hemin content. As indicated by Neves-Petersen et al. (2007), in peroxidases, in fact, the catalytic activity is dependent on the presence and correct conformation of the heme moiety and the residues forming the catalytic pocket, and the Rz reduction suggests an alteration at the level of the heme cavity. Increasing the exposition of HRP to CAP, a linear decrease (r=0.889) in the Rz value was determined (data not shown); in particular, the HRP treated for 30 min showed an Rz of 0.93±0.004 vs 2.02±0.003 of the untreated protein, indicating that more than 50% of the heme moiety was modified by CAP treatment. This kind of effect was also found in previous research investigating the effects of cold plasma and other treatments, such as guanidinium chloride, pH, heat, UV, and pulsed light on the HRP activity and structure (S. Dong et al., 2021; Y. X. Han et al., 2019; Pellicer & Gómez-López, 2017; Y. Wang et al., 2021).

3.2.4 Fluorescence spectroscopy analysis

Since tryptophan and tyrosine fluorescence give useful information to detect possible changes both in the tertiary structure of the protein and the polarity of the Trp and Tyr microenvironment, fluorescence emission spectra (λ_{ex} = 280 and 330 nm) of the HRP buffered systems were collected before and after different CAP exposition times (Fig. 5a-5b).

The fluorescence spectrum of the native enzyme at λ_{ex} = 280 (Fig. 5a) was characterized by a peak at 336 nm in agreement with what was reported by Surowsky et al. (2013). After CAP exposure, a slight blue shift of the fluorescence peak was observed, as well as a decrease in the maximum fluorescence intensity (I_{max}), and the extent of these phenomena increased with the increase of the CAP exposure time. In particular, after 30 min of exposure, the maximum intensity shifted from 336 nm to 328 nm. Fluorescence quenching after CAP exposure was also highlighted by other authors (Surowsky et al., 2013; Y. Wang et al., 2021) and is possibly ascribed to i) the attack of reactive species produced by cold plasma on aromatic amino acids; ii) a decrease of the distance between tryptophan and the heme group that could cause the energy transfer from tryptophan to the heme (Surowsky et al., 2013); iii) the burial of the fluorophores in the core of proteins due to the folding of the molecular chains. This last hypothesis would explain the blue shift of the maximum fluorescent intensity since the tryptophan residues situated in the core of proteins emit light in lower wavelength regions than those located at the surface (Burstein et al., 1973). In order to highlight the role of these modifications on the HRP activity, the Pearson correlation test was performed using I_{max} and HRP activity data as variables, and a high coefficient of correlation (r= 0.923) was found. This result indicates that the modifications impaired by CAP on aromatic amino acids influence the HRP activity.

The fluorescence changes of HRP with the excitation wavelength at 330 nm were also investigated to get information on the heme degradation (Ke & Huang, 2013). As shown in Fig. 5b, the spectrum of the native protein showed a small peak at around 425 nm that, after CAP treatments, increased with no λ_{em} shift because of the production of fluorescent products formed in HRP solution originating from heme destruction. This result may explain what was also highlighted by UV-Vis analyses, i.e., heme located at the active site of HRP upon CAP treatments reacts with ozone and its degradation reaction products such as H_2O_2 producing fluorescence heme degradation products (S. Dong et al., 2021; Ke & Huang, 2013; Nagababu & Rifkind, 1998; Y. Wang et al., 2021). To understand the role of this change on the HRP activity, the Pearson correlation test was carried out using I_{max} (after excitation at 330 nm) and HRP activity as variables, and a high coefficient of correlation (r= 0.852) was found, indicating that the modifications impaired by CAP the heme moiety negatively affected the HRP activity.

Based on these results, in agreement with what was reported by other authors (Y. X. Han et al., 2019; Surowsky et al., 2013; Y. Wang et al., 2021), it can be assumed that the loss of enzyme activity highlighted after CAP treatments is due to the modification of the HRP tertiary structure and heme degradation.

3.2.5. CD spectra analysis

CD spectroscopy measures the differential absorption of left- and right-circularly polarised light by chiral molecules such as proteins. The resulting CD spectra provide information about the types and amounts of secondary structures present in the protein. Specifically, the CD spectrum in the far-UV range (190-250 nm) is particularly sensitive to the secondary structure of proteins because it reflects the absorption of the peptide bond chromophore. In Fig. 6a the far UV CD (200-260 nm) spectra of treated and untreated HRP, expressed in terms of residual ellipticity, are reported. The CD spectra of the untreated HRP exhibit the characteristic negative peaks at 208 nm and 222 nm and the shoulder at 218 nm, indicating, respectively, the presence of alpha-helical and beta-sheet structures. These findings are consistent with the known secondary structure of HRP, which is predominantly composed of alpha-helices and beta-sheets (Surowsky et al., 2013; Y. Wang et al., 2021; Zhong et al., 2005). After plasma exposure, the spectra show a decrease in the negative peak at 208 nm and the shoulder at 218 nm, implying a decline in alpha-helical structure and a rise in beta-sheet content. More specifically, as highlighted by the deconvolution of CD spectra, after 30 minutes of plasma exposure, alpha helices decreased by 5 percentage points while that beta sheets (including both parallel and antiparallel) increased by 3 percentage points. These results contribute to explaining the loss of activity highlighted after CAP treatment and confirm the findings of other authors (Y. X. Han et al., 2019; Surowsky et al., 2013; Y. Wang et al., 2021) on the capability of cold plasma processing to change the conformational structure of proteins. However, comparing the relative content before and after processing with those reported in the overmentioned literature, it is also worth noting that the variation of alpha-helices and beta-sheet induced by cold plasma processing on HRP vary depending on the specific peroxidase being treated and the specific plasma treatment conditions, i.e., configuration, type of gas, gas flow rate, treatment time, power. All these factors, in turn, affect the plasma composition and the type of structural damage. In a complex plasma, in fact, many reactions can cause conformational and secondary structural changes, but all of them are likely initiated by the inherent radical species (RS). These RS can cleave peptide bonds and modify amino acid chains thereby producing secondary structure changes. The sulfur-containing amino acids such as cysteine and aromatic amino acids are particularly susceptible (Zhang et al., 2015).

3.3 Inactivation and structural changes of HRP in sugar model systems induced by CAP treatments

3.3.1 HRP inactivation

To highlight the effects induced by CAP treatments on HRP in sugar model systems, the first step of the investigation was aimed at determining possible effects induced by the different co-solutes on the enzyme activity. As shown in Fig. 7, all the sugar negatively affected the HRP activity, and this effect was influenced both by the sugar concentration and type. In particular, by comparing the HRP activity of sugar samples characterized by equal sugar molality (systems G1, F1, S1, and T1), a similar ($p<0.05$) inhibition percentage (about 26%) was observed for glucose, fructose, and sucrose while trehalose resulted in the most effective with an HRP reduction of about 38%. However, when the HRP activity was measured on samples characterized by a higher sugar concentration (G2, F2, S2, and T2), very different results were obtained among the sugars, and only for glucose and sucrose at the increase of the sugar concentration corresponded a decrease of the HRP activity. Since the determination of the enzyme activity required a strong dilution of the sample (1:53), these results are possibly due to sugar/protein interactions and quenching of ABTS radical by sugars rather than environmental physical and physicochemical changes induced by the sugars in the aqueous phase.

On this basis, for each sugar model system, the residual activity of HRP after cold plasma treatments was expressed as the percentage ratio between the reaction rate after cold plasma treatment and the absorption rate measured on the corresponding untreated sample. Fig. 7 reported the HRP inactivation kinetics obtained for the different sugar model systems. The results clearly indicate a protective effect of sugars on HRP inactivation by CAP. Irrespective of the CAP exposure time, all the sugar model systems showed a higher HRP residual activity compared to the enzyme in PBS. However, by comparing the inactivation kinetics of the systems containing mono- and disaccharides some differences could be noted. In particular, at equal molality, glucose (G1) showed a higher protective effect than fructose (F1) (Fig. 8a-8b), and both the monosaccharides showed a lower capacity to protect HRP compared to sucrose (S1) and trehalose (T1) (Fig. 8c-8d). These results are due to the ability of sugars, and especially of disaccharides, to scavenge free radicals (Li et al., 2014; Morelli et al., 2003) with a concentration-dependent effect (Surowsky et al., 2016). Moreover, these solutes act as kosmotropes (water structure-forming factor) and, depending on their concentration and type, are preferentially or weaky excluded from the protein surface and prevent denaturation phenomena through the suppression of perturbation of the hydration structure of the protein. In particular, Hirai (2020) and Ajito et al. (2018) showed that glucose and fructose can protect the protein by preserving their native hydration shell for concentrations lower than about 25 and 16% (w/v), respectively, while at higher concentrations the preferential exclusion shifts to neutral and preferential solvation.

Conversely, for sucrose and trehalose, this shift occurs at higher concentrations (about 28% w/v for sucrose and 37% w/v for trehalose). Thus, based on the sugar concentrations investigated in this study, it can be hypothesized that the differences highlighted in the protective effect of the sugars toward HRP activity were also dependent on differences in the HRP hydration shell. Finally, the highest viscosity of the disaccharide systems (table S1) could have played a role in the HRP inactivation by cold plasma reactive species by reducing their mobility in the system.

3.3.2 Absorption spectra

To understand the mechanisms of protection of sugars on HRP upon CAP exposure, UV-Vis absorption spectra of HRP sugar model systems before and after treatments were collected (Fig. 9). By comparing the spectra of the untreated samples with that of HRP in PBS, it can be noted that all the sugars, irrespective to their concentration, affected the native state of the protein. In particular, glucose and fructose provoked the strongest modification determining respectively an increase and a decrease of the absorbance at 275 nm, possibly ascribed to i) the change of the exposition of aromatic amino acids to the protein environment, ii) the decrease and red-shift (of 6 nm for G1 and G2 systems and 15 nm for F1 and F2) of the Soret band, and iii) the disappearance of the charge transfer transitions (CT1, 498 nm) characteristic of a pentacoordinate state of the iron (Neves-Petersen et al., 2007) and formation of two Q-bands at 527 nm and 557 nm indicating the generation of ferryl intermediates of HRP (Ravanfar & Abbaspourrad, 2021). Conversely, disaccharides determined solely a change of the maximum absorbance at 275 nm and 403 nm, which was higher for samples S1, S2, and T2 and slightly lower for T1.

In all the sugar model systems, CAP exposure determined a loss of the peak at 275 nm and a reduction of the Soret and Q bands, and the extent of these modifications was time-dependent and always lower than that observed in PBS. This result indicates a protective effect of sugars on the protein tertiary structure. Similar results were also obtained by Ajito et al. (2018) upon the chemical denaturation of myoglobin, a heme-containing protein. According to what was highlighted by other authors (Ke & Huang, 2013), the modifications observed on the Soret band and of the peak at 275 nm due to CAP treatments were involved in the changes in the HRP activity. Indeed, by calculating the Rz (Abs_{430}/Abs_{275}) for all the sugar model systems characterized by an HRP activity reduction, (all except S2 and T2) and correlating them to the HRP activity, a significant correlation was found (Fig. 10). However, comparing mono- and disaccharides, it was found that the dependence of the HRP activity on the Rz was higher for the former and lower for the latter. Finally, comparing the dataset of both the sugar systems with that of PBS (Fig. 10), a lower dependence and correlation of HRP activity to the Rz was found. These results indicate that in sugar systems, conformational changes induced by CAP on HRP are not the sole factor affecting the enzyme activity and that sugar antiradical

activity (disaccharides > monosaccharides) and capacity to preserve the protein hydration shell seems to play a role in the HRP inactivation.

3.3.3 Fluorescence spectroscopy analysis

To insight into the conformational modifications induced by the CAP treatments on HRP in sugar model systems, fluorescence emission spectra after excitation at 280 nm were collected. By comparing the spectra of the untreated samples with that of the native protein (Table 1), it can be observed that monosaccharides decreased the HRP fluorescent emission with no λ shift. This effect was concentration-dependent and more pronounced for fructose. Trehalose had the same effect only at the lowest concentration, while at the highest concentration, it determined only a red shift of 2 nm. Conversely, with increasing sucrose concentration, both an increase in the HRP fluorescence emission intensity (up to 37%) and a red shift of the peak (up to 12 nm) were observed. However, these results are due to the interference of sucrose on the HRP fluoresce emission spectra.

As observed for the PBS system, after CAP in all the HRP sugar systems, a blue shift of the fluorescence peak was observed, as well as a decrease of the maximum fluorescence intensity (I_{max}), and the extent of these phenomena increased with the increase of the CAP exposure. As previously explained, these phenomena are possibly ascribed to the oxidation by plasma reactive species of aromatic amino acids and/or the burial of the fluorophores in the core of proteins due to the folding of the molecular chains. However, compared to PBS, on percentage, the I_{max} decrease due to CAP resulted lower ($p<0.05$) in the systems containing monosaccharides or trehalose irrespective of their concentration; conversely, in the sucrose systems, it resulted higher or like that observed for PBS systems depending on the CAP exposure times.

To evaluate any correlation between the I_{max} modifications and the HRP inactivation induced by CAP, the Pearson correlation test and linear regression were performed on the data set of systems showing HRP reduction (all except S2 and T2) (Table 2). The correlation (r) was significant for each sugar system, however, molality being equal (G1, F1, S1, T1), a higher dependence (about one order magnitude) of HRP activity on I_{max} was observed in PBS and monosaccharides systems than in disaccharide ones (S1 and T1). This result implies that the inactivation of HRP induced by CAP in disaccharide systems was less dependent on the phenomena affecting aromatic amino acids.

The fluorescence emission spectra of HRP at 425 nm after excitation at 330 nm were also investigated to get information on the heme degradation (data not shown). The addition of sugars to HRP determined a slight increase in the fluorescence emission that was sugar- and concentration-dependent.

After CAP treatment, it was observed an increase in the fluorescence intensity ascribable to the production of fluorescence heme degradation products only in the HRP systems containing glucose

476 or fructose and only for CAP exposure times higher than 10 min (data not shown). These results
477 suggest a possible protective effect of disaccharides on the heme moiety due to their capability to
478 quench plasma reactive species and stabilize the HRP native structure.

479 **3.3.4 CD spectra analysis**

480 To highlight the modifications induced by CAP treatments on the secondary structure of the HRP in
481 sugar model systems, CD spectra of the sugar model systems characterized by equal molality were
482 collected before and after CAP for 30 min. CD spectra deconvolution by CDNN software was
483 performed to determine the contents of secondary structures (Fig. 11).
484 Upon comparing the untreated samples with the native protein, it can be observed that all the sugars
485 (F1>S1>T1>G1) influenced the secondary structure of the HRP, determining an increase in the alpha-
486 helices. As regards beta sheets, they decreased in F1 and S1 and slightly increased in T1 and G1. This
487 result indicates that the interaction of sugars with HRP induced, overall, a more ordered secondary
488 structure.
489 After plasma exposure, a reduction of alpha-helices was highlighted on T1 and to a lower extent on
490 G1, however, only for G1 was accompanied by a decrease in beta-sheets, likewise in PBS. As regards
491 the S1 and F1 systems, CAP determined an increase in alpha-helices and a decrease in beta-sheets.
492 Overall, the HRP native secondary structure was best preserved in G1 and T1 systems. These results
493 contribute to explaining the stabilizing effect of trehalose on HRP activity even at low concentrations
494 (T1).
495

496 **4. Conclusions**

497 This study deepened the knowledge on the effect of SDBD cold atmospheric plasma on HRP activity
498 providing information on the role played by sugars on the enzyme inactivation.
499 In the PBS system, CAP treatments significantly reduced the HRP activity, and the extent of the
500 inactivation was dependent on processing time and ozone concentration in the treatment chamber.
501 Spectroscopic techniques highlighted that the loss of the HRP activity was due to changes in protein
502 tertiary structure and loss of secondary (alpha-helices) structures.
503 Sugars significantly reduced the inactivation of HRP by CAP and this effect was concentration-
504 dependent and higher for disaccharides than for monosaccharides. Studies on the HRP tertiary and
505 secondary structure suggested that the protective effect of sugars was not only due to their capability
506 to preserve the enzyme conformation but was possibly related to their different ability to quench
507 plasma reactive species (disaccharides > monosaccharides) and to stabilize the protein by preserving
508 its hydration shell. Finally, the highest viscosity of the sugar model systems could have played a role
509 in the HRP inactivation by cold plasma reactive species by reducing their mobility in the system.

Declaration of Conflict of Interest

The authors declare no conflict of interest.

Funding

The present work is part of the research activities developed within the project "PLASMAFOOD—Study and optimisation of cold atmospheric plasma treatment for food safety and quality improvement" founded by MIUR—Ministero dell'Istruzione dell'Università e della Ricerca—PRIN: Progetti di Ricerca di Rilevante Interesse Nazionale, Bando 2017.

References

Adams, J. B. (1991). Review: Enzyme inactivation during heat processing of food-stuffs. International Journal of Food Science & Technology, 26(1), 1–20. https://doi.org/10.1111/J.1365-2621.1991.TB01136.X

Ajito, S., Iwase, H., Takata, S. I., & Hirai, M. (2018). Sugar-Mediated Stabilization of Protein against Chemical or Thermal Denaturation. Journal of Physical Chemistry B, 122(37), 8685–8697. https://doi.org/10.1021/acs.jpcb.8b06572

Arakawa, T., & Timasheff, S. N. (1982). Stabilization of Protein Structure by Sugars. Biochemistry, 21(25), 6536–6544. https://doi.org/10.1021/BI00268A033/ASSET/BI00268A033.FP.PNG_V03

Barbiroli, A., Marengo, M., Fessas, D., Ragg, E., Renzetti, S., Bonomi, F., & Iametti, S. (2017). Stabilization of beta-lactoglobulin by polyols and sugars against temperature-induced denaturation involves diverse and specific structural regions of the protein. Food Chemistry, 234, 155–162. https://doi.org/10.1016/j.foodchem.2017.04.132

Burnette, F. S. (1977). Peroxidase and its relationship to food flavor and quality: a review. Journal of Food Science, 42(1), 1–6. https://doi.org/10.1111/J.1365-2621.1977.TB01204.X

Burstein, E. A., Vedenkina, N. S., & Ivkova, M. N. (1973). Fluorescence and the location of tryptophan residues in protein molecules. Photochemistry and Photobiology, 18(4), 263–279. https://doi.org/10.1111/J.1751-1097.1973.TB06422.X

538 Chattopadhyay, K., & Mazumdar, S. (1999). Structural and Conformational Stability of Horseradish
539 Peroxidase: Effect of Temperature and pH. Biochemistry, 39(1), 263–270.
540 https://doi.org/10.1021/BI990729O

541 Chutia, H., Kalita, D., Mahanta, C. L., Ojah, N., & Choudhury, A. J. (2019). Kinetics of inactivation
542 of peroxidase and polyphenol oxidase in tender coconut water by dielectric barrier discharge plasma.
543 Lwt, 101, 625–629. https://doi.org/10.1016/j.lwt.2018.11.071

544 Corezzi, S., Bracco, B., Sassi, P., Paolantoni, M., & Comez, L. (2021). Protein hydration in a
545 bioprotecting mixture. Life, 11(10), 995. https://doi.org/10.3390/life11100995

546 De Fátima Machado, M., Oliveira, F. A. R., Gekas, V., & Singh, R. P. (1998). Kinetics of moisture
547 uptake and soluble-solids loss by puffed breakfast cereals immersed in water. International Journal
548 of Food Science & Technology, 33(3), 225–237. https://doi.org/10.1046/J.1365-2621.1998.00197.X

549 De Flaviis, R., & Sacchetti, G. (2022). Reparameterization of the Weibull model for practical uses in
550 food science. Journal of Food Science, 87(5), 2096–2111. https://doi.org/10.1111/1750-3841.16124

551 Dharini, M., Jaspin, S., & Mahendran, R. (2023). Cold plasma reactive species: Generation,
552 properties, and interaction with food biomolecules. Food Chemistry, 405(Part A).
553 https://doi.org/10.1016/J.FOODCHEM.2022.134746

554 Dong, S., Fan, L., Ma, Y., Du, J., & Xiang, Q. (2021). Inactivation of polyphenol oxidase by dielectric
555 barrier discharge (DBD) plasma: Kinetics and mechanisms. Lwt, 145(136), 111322.
556 https://doi.org/10.1016/j.lwt.2021.111322

557 Dong, X. Y., & Yang, Y. L. (2019). A Novel Approach to Enhance Blueberry Quality During Storage
558 Using Cold Plasma at Atmospheric Air Pressure. Food and Bioprocess Technology, 12(8), 1409–
559 1421. https://doi.org/10.1007/s11947-019-02305-y

560 Ekezie, F. G. C., Cheng, J. H., & Sun, D. W. (2019). Effects of atmospheric pressure plasma jet on
561 the conformation and physicochemical properties of myofibrillar proteins from king prawn
562 (Litopenaeus vannamei). Food Chemistry, 276, 147–156.
563 https://doi.org/10.1016/J.FOODCHEM.2018.09.113

564 Faieta, M., Neri, L., Di Michele, A., Di Mattia, C. D., & Pittia, P. (2021). High hydrostatic pressure
565 treatment of Arthrospira (Spirulina) platensis extracts and the baroprotective effect of sugars on

566 phycobiliproteins. Innovative Food Science & Emerging Technologies, 70, 102693.
567 https://doi.org/10.1016/J.IFSET.2021.102693

568 Faieta, M., Neri, L., Sacchetti, G., Di Michele, A., & Pittia, P. (2020). Role of saccharides on thermal
569 stability of phycocyanin in aqueous solutions. Food Research International, 132, 109093.
570 https://doi.org/10.1016/j.foodres.2020.109093

571 Fernandes, F. A. N., & Rodrigues, S. (2021). Cold plasma processing on fruits and fruit juices: A
572 review on the effects of plasma on nutritional quality. Processes, 9(12).
573 https://doi.org/10.3390/pr9122098

574 Gui, F., Chen, F., Wu, J., Wang, Z., Liao, X., & Hu, X. (2006). Inactivation and structural change of
575 horseradish peroxidase treated with supercritical carbon dioxide. Food Chemistry, 97(3), 480–489.
576 https://doi.org/10.1016/J.FOODCHEM.2005.05.028

577 Han, Y., Cheng, J. H., & Sun, D. W. (2019). Activities and conformation changes of food enzymes
578 induced by cold plasma: A review. Critical Reviews in Food Science and Nutrition, 59(5), 794–811.
579 https://doi.org/10.1080/10408398.2018.1555131

580 Han, Y. X., Cheng, J. H., & Sun, D. W. (2019). Changes in activity, structure and morphology of
581 horseradish peroxidase induced by cold plasma. Food Chemistry, 301, 125240.
582 https://doi.org/10.1016/j.foodchem.2019.125240

583 Hirai, M. (2020). Sugars can protect hydration shell of proteins and stabilize their native structures in
584 crowded molecular environment: clarified by complemental use of X-rays and neutrons. SPring-
585 8/SACLA Research Frontiers, 23, 13–14. http://www.spring8.or.jp/pdf/en/res_fro/19/024-025.pdf

586 Hollósy, F. (2002). Effects of ultraviolet radiation on plant cells. Micron, 33(2), 179–197.
587 https://doi.org/10.1016/S0968-4328(01)00011-7

588 Jang, J. H., & Moon, K. D. (2011). Inhibition of polyphenol oxidase and peroxidase activities on
589 fresh-cut apple by simultaneous treatment of ultrasound and ascorbic acid. Food Chemistry, 124(2),
590 444–449. https://doi.org/10.1016/J.FOODCHEM.2010.06.052

591 Ke, Z., & Huang, Q. (2013). Inactivation and Heme Degradation of Horseradish Peroxidase Induced
592 by Discharge Plasma. Plasma Processes and Polymers, 10(8), 731–739.
593 https://doi.org/10.1002/PPAP.201300035

Keesey, J. (1987). Biochemica Information: A revised biochemical reference source. Boehringer Mannheim Biochemicals.

Lee, J. C., & Timasheff, S. N. (1981). The stabilization of proteins by sucrose. Journal of Biological Chemistry, 256(14), 7193–7201. https://doi.org/10.1016/S0021-9258(19)68947-7

Li, Y., Friedman, G., Fridman, A., & Ji, H. F. (2014). Decomposition of sugars under non-thermal dielectric barrier discharge plasma. Clinical Plasma Medicine, 2(2), 56–63. https://doi.org/10.1016/j.cpme.2014.08.001

Lo'ay, A. A., & Dawood, H. D. (2017). Minimize browning incidence of banana by postharvest active chitosan/PVA Combines with oxalic acid treatment to during shelf-life. Scientia Horticulturae, 226, 208–215. https://doi.org/10.1016/J.SCIENTA.2017.08.046

Matsui, K. N., Granado, L. M., de Oliveira, P. v., & Tadini, C. C. (2007). Peroxidase and polyphenol oxidase thermal inactivation by microwaves in green coconut water simulated solutions. LWT - Food Science and Technology, 40(5), 852–859. https://doi.org/10.1016/J.LWT.2006.03.019

Mir, S. A., Shah, M. A., & Mir, M. M. (2016). Understanding the Role of Plasma Technology in Food Industry. Food and Bioprocess Technology, 9(5), 734–750. https://doi.org/10.1007/S11947-016-1699-9

Misra, N. N., Pankaj, S. K., Segat, A., & Ishikawa, K. (2016). Cold plasma interactions with enzymes in foods and model systems. Trends in Food Science and Technology, 55, 39–47. https://doi.org/10.1016/j.tifs.2016.07.001

Molina-Hernandez, J. B., Laika, J., Peralta-Ruiz, Y., Palivala, V. K., Tappi, S., Cappelli, F., Ricci, A., Neri, L., & Chaves-López, C. (2022). Influence of Atmospheric Cold Plasma Exposure on Naturally Present Fungal Spores and Physicochemical Characteristics of Sundried Tomatoes (Solanum lycopersicum L.). Foods, 11(2). https://doi.org/10.3390/foods11020210

Morelli, R., Russo-Volpe, S., Bruno, N., & Lo Scalzo, R. (2003). Fenton-Dependent Damage to Carbohydrates: Free Radical Scavenging Activity of Some Simple Sugars. Journal of Agricultural and Food Chemistry, 51(25), 7418–7425. https://doi.org/10.1021/jf030172q

620 Nagababu, E., & Rifkind, J. M. (1998). Formation of Fluorescent Heme Degradation Products during
621 the Oxidation of Hemoglobin by Hydrogen Peroxide. Biochemical and Biophysical Research
622 Communications, 247(3), 592–596. https://doi.org/10.1006/BBRC.1998.8846

623 Neves-Petersen, M. T., Klitgaard, S., Carvalho, A. S. L., Petersen, S. B., De Barros, M. R. A., & E
624 Meloz, E. P. (2007). Photophysics and photochemistry of horseradish peroxidase A2 upon ultraviolet
625 illumination. Biophysical Journal, 92(6), 2016–2027. https://doi.org/10.1529/biophysj.106.095455

626 Pan, Y., Cheng, J. H., & Sun, D. W. (2019). Cold Plasma-Mediated Treatments for Shelf Life
627 Extension of Fresh Produce: A Review of Recent Research Developments. Comprehensive Reviews
628 in Food Science and Food Safety, 18(5), 1312–1326. https://doi.org/10.1111/1541-4337.12474

629 Pankaj, S. K., Misra, N. N., & Cullen, P. J. (2013). Kinetics of tomato peroxidase inactivation by
630 atmospheric pressure cold plasma based on dielectric barrier discharge. Innovative Food Science and
631 Emerging Technologies, 19, 153–157. https://doi.org/10.1016/j.ifset.2013.03.001

632 Pavlovich, M. J., Clark, D. S., & Graves, D. B. (2014). Quantification of air plasma chemistry for
633 surface disinfection. Plasma Sources Science and Technology, 23(6), 65036.
634 https://doi.org/doi:10.1088/0963-0252/23/6/065036

635 Peleg, M. (1988). An Empirical Model for the Description of Moisture Sorption Curves. Journal of
636 Food Science, 53(4), 1216–1217. https://doi.org/10.1111/J.1365-2621.1988.TB13565.X

637 Pellicer, J. A., & Gómez-López, V. M. (2017). Pulsed light inactivation of horseradish peroxidase
638 and associated structural changes. Food Chemistry, 237, 632–637.
639 https://doi.org/10.1016/j.foodchem.2017.05.151

640 Pizzocaro, F., Aggujaro, R., & Bertolo, G. (1994). Kinetics of enzymes inactivation in carrot disks
641 during blanching. Rivista Di Scienza Dell'Alimentazione (Italy), 22(3), 279–285.

642 Préstamo, G., Arabas, J., Fonberg-Broczek, M., & Arroyo, G. (2001). Reaction of B. cereus Bacteria
643 and Peroxidase Enzymes under Pressures >400 MPa. Journal of Agricultural and Food Chemistry,
644 49(6), 2830–2834. https://doi.org/10.1021/JF001013Z

645 Punia Bangar, S., Suri, S., Nayi, P., & Phimolsiripol, Y. (2022). Cold plasma for microbial safety:
646 Principle, mechanism, and factors responsible. Journal of Food Processing and Preservation, 46(12),
647 e16850. https://doi.org/10.1111/JFPP.16850

Ravanfar, R., & Abbaspourrad, A. (2021). Monitoring the heme iron state in horseradish peroxidase to detect ultratrace amounts of hydrogen peroxide in alcohols. RSC Advances, 11(17), 9901–9910. https://doi.org/10.1039/D1RA00733E

Richter Reis, F. (2023). Blanching in the food industry. In Thermal Processing of Food Products by Steam and Hot Water (pp. 211–246). Woodhead Publishing. https://doi.org/10.1016/B978-0-12-818616-9.00007-9

Sacchetti, G., Pittia, P., & Pinnavaia G.G. (2005). The effect of extrusion temperature and drying-tempering on both the kinetics of hydration and the textural changes in extruded ready- to- eat breakfast cereals during soaking in semi- skimmed milk. International Journal of Food Science & Technology, 40(6),655–663. https://doi.org 10.1111/j.1365-2621.2005.00976.x

Sarangapani, C., Patange, A., Bourke, P., Keener, K., & Cullen, P. J. (2018). Recent Advances in the Application of Cold Plasma Technology in Foods. Annual Review of Food Science and Technology, 9, 609–629. https://doi.org/10.1146/annurev-food-030117-012517

Sola-Penna, M., Ferreira-Pereira, A., Lemos, A. D. P., & Meyer-Fernandes, J. R. (1997). Carbohydrate Protection of Enzyme Structure and Function against Guanidinium Chloride Treatment Depends on the Nature of Carbohydrate and Enzyme. European Journal of Biochemistry, 248(1), 24–29. https://doi.org/10.1111/J.1432-1033.1997.00024.X

Sola-Penna, M., & Meyer-Fernandes, J. R. (1994). Protective role of trehalose in thermal denaturation of yeast pyrophosphatase. Zeitschrift Fur Naturforschung. C, Journal of Biosciences, 49(5–6), 327–330. https://doi.org/https://doi.org/10.1515/znc-1994-5-608

Sola-Penna, M., & Meyer-Fernandes, J. R. (1998). Stabilization against thermal inactivation promoted by sugars on enzyme structure and function: Why is trehalose more effective than other sugars? Archives of Biochemistry and Biophysics, 360(1), 10–14. https://doi.org/10.1006/abbi.1998.0906

Surowsky, B., Bußler, S., & Schlüter, O. K. (2016). Cold Plasma Interactions With Food Constituents in Liquid and Solid Food Matrices. Cold Plasma in Food and Agriculture: Fundamentals and Applications, 179–203. https://doi.org/10.1016/B978-0-12-801365-6.00007-X

675 Surowsky, B., Fischer, A., Schlueter, O., & Knorr, D. (2013). Cold plasma effects on enzyme activity
676 in a model food system. Innovative Food Science and Emerging Technologies, 19, 146–152.
677 https://doi.org/10.1016/j.ifset.2013.04.002

678 Tappi, S., Berardinelli, A., Ragni, L., Dalla Rosa, M., Guarnieri, A., & Rocculi, P. (2014).
679 Atmospheric gas plasma treatment of fresh-cut apples. Innovative Food Science & Emerging
680 Technologies, 21, 114–122. https://doi.org/10.1016/J.IFSET.2013.09.012

681 Tappi, S., Gozzi, G., Vannini, L., Berardinelli, A., Romani, S., Ragni, L., & Rocculi, P. (2016). Cold
682 plasma treatment for fresh-cut melon stabilization. Innovative Food Science & Emerging
683 Technologies, 33, 225–233. https://doi.org/10.1016/J.IFSET.2015.12.022

684 Thirumdas, R., & Annapure, U. S. (2020). Enzyme inactivation in model systems and food matrixes
685 by cold plasma. In Advances in Cold Plasma Applications for Food Safety and Preservation (pp. 229–
686 252). Academic Press. https://doi.org/10.1016/B978-0-12-814921-8.00007-4

687 Tijskens, L. M. M., Waldron, K. W., Ng, A., Ingham, L., & Van Dijk, C. (1997). The kinetics of
688 pectin methyl esterase in potatoes and carrots during blanching. Journal of Food Engineering, 34(4),
689 371–385. https://doi.org/10.1016/S0260-8774(98)00005-3

690 Timasheff, S. N. (1993). The control of protein stability and association by weak interactions with
691 water: how do solvents affect these processes? Annual Review of Biophysics and Biomolecular
692 Structure, 22, 67–97. https://doi.org/https://doi.org/10.1146/annurev.bb.22.060193.000435

693 Tsouvaltzis, P., & Brecht, J. K. (2017). Inhibition of Enzymatic Browning of Fresh-Cut Potato by
694 Immersion in Citric Acid is Not Solely Due to pH Reduction of the Solution. Journal of Food
695 Processing and Preservation, 41(2), e12829. https://doi.org/10.1111/JFPP.12829

696 Wang, B., Zhang, Y., Venkitasamy, C., Wu, B., Pan, Z., & Ma, H. (2017). Effect of pulsed light on
697 activity and structural changes of horseradish peroxidase. Food Chemistry, 234, 20–25.
698 https://doi.org/10.1016/J.FOODCHEM.2017.04.149

699 Wang, Y., Ye, Z., Li, J., Zhang, Y., Guo, Y., & Cheng, J. H. (2021). Effects of dielectric barrier
700 discharge cold plasma on the activity, structure and conformation of horseradish peroxidase (HRP)
701 and on the activity of litchi peroxidase (POD). Lwt, 141, 111078.
702 https://doi.org/10.1016/j.lwt.2021.111078

703 Zhang, H., Xu, Z., Shen, J., Li, X., Ding, L., Ma, J., Lan, Y., Xia, W., Cheng, C., Sun, Q., Zhang, Z.,
704 & Chu, P. K. (2015). Effects and Mechanism of Atmospheric-Pressure Dielectric Barrier Discharge
705 Cold Plasma on Lactate Dehydrogenase (LDH) Enzyme. Scientific Reports , 5(1), 10031.
706 https://doi.org/https://doi.org/10.1038/srep10031

707 Zhong, K., Hu, X., Zhao, G., Chen, F., & Liao, X. (2005). Inactivation and conformational change of
708 horseradish peroxidase induced by pulsed electric field. Food Chemistry, 92(3), 473–479.
709 https://doi.org/10.1016/j.foodchem.2004.08.010

710

Declaration of Conflict of Interest

The authors declare no conflict of interest.

Author Statement

Jessica Laika*:** Investigation, Formal analysis, Visualization, Writing- Original draft preparation, Writing- Reviewing and Editing. ***Giampiero Sacchetti: Conceptualization, Methodology, Formal analysis, Writing- Original draft preparation, Writing- Reviewing and Editing. ***Annalaura Sabatucci:*** Methodology**,** Investigation, Visualization, Writing- Original draft preparation. ***Junior Bernardo Molina-Hernandez:*** Investigation, Visualization. ***Antonella Ricci:*** Methodology. ***Romolo Laurita:*** Methodology**,** Investigation. ***Silvia Tappi:*** investigation. ***Alessandro Di Michele:*** Investigation. ***Lilia Neri:*** Supervision, Conceptualization, Methodology, Formal analysis, Writing- Original draft preparation, Writing- Reviewing and Editing.

Figure captions

Fig. 1. O_3 concentration measured in the treatment chamber over time. The insert shows the parameters calculated fitting the data with the Peleg equation.

Fig. 2. HRP inactivation kinetic in PBS system. Values are presented as means ± standard deviations (n=3). Values with different superscripted letters are significantly different ($p < 0.05$).

Fig. 3. First order and Weibull model curve fitting of HRP inactivation in PBS system as a function of the CAP exposure time **(a);** the related estimated kinetic parameters are shown in the insert. Weibull model curve fitting of HRP inactivation in PBS system as a function of the O_3 concentration **(b);** the related estimated kinetic parameters are shown in the insert

Fig. 4. UV-Vis absorption spectra of HRP in buffered systems before and after different CAP exposure times (5, 10, 20, 30 min).

Fig. 5. Fluorescence emission spectra of the HRP buffered system before and after different CAP exposure times (5, 10, 20, 30 min); **(a)** λex = 280 and **(b)** λex = 330 nm.

Fig. 6. Effect of CAP treatment on the secondary structure of HRP in PBS system before and after 30 min of treatment. **(a)** Relative content of α-helix, β-sheet, unfolded structures, and turns as determined by CDNN software. **(b)** Far-UV CD spectra.

Fig. 7. Effect of sugars at two different concentrations on HRP enzymatic activity (untreated samples). Values are presented as means ± standard deviations (n=3). Values with different superscripted letters are significantly different ($p < 0.05$).

Fig. 8. HRP inactivation kinetic in PBS system and sugar model systems. **(a)** glucose, **(b)** fructose, **(c)** sucrose, **(d)** trehalose. Values are presented as means ± standard deviations (n=3). Values with different superscripted letters are significantly different ($p < 0.05$).

Fig. 9. UV-Vis absorption spectra of HRP in different sugar model systems before and after different CAP exposure times (5, 10, 20, 30 min): **(a-b)** glucose, **(c-d)** fructose, **(e-f)** sucrose, **(g-h)** trehalose.

Fig. 10. HRP activity ($\Delta A\ min^{-1}$) detected in all monosaccharide (G1, G2, F1, F2) and disaccharide (S1, T1) systems treated by CAP expressed as a function of the corresponding Rz (Abs_{403}/Abs_{275}) values.

Fig. 11. Effect of CAP treatment on the secondary structure of HRP in PBS system and sugar systems characterized by equal molality before and after 30 min of CAP treatment. Bars show the relative content of α-helix, β-sheet, unfolded structures, and turns as determined by CDNN software.

Figure 1

Click here to access/download;Figure;Figure 1.pdf

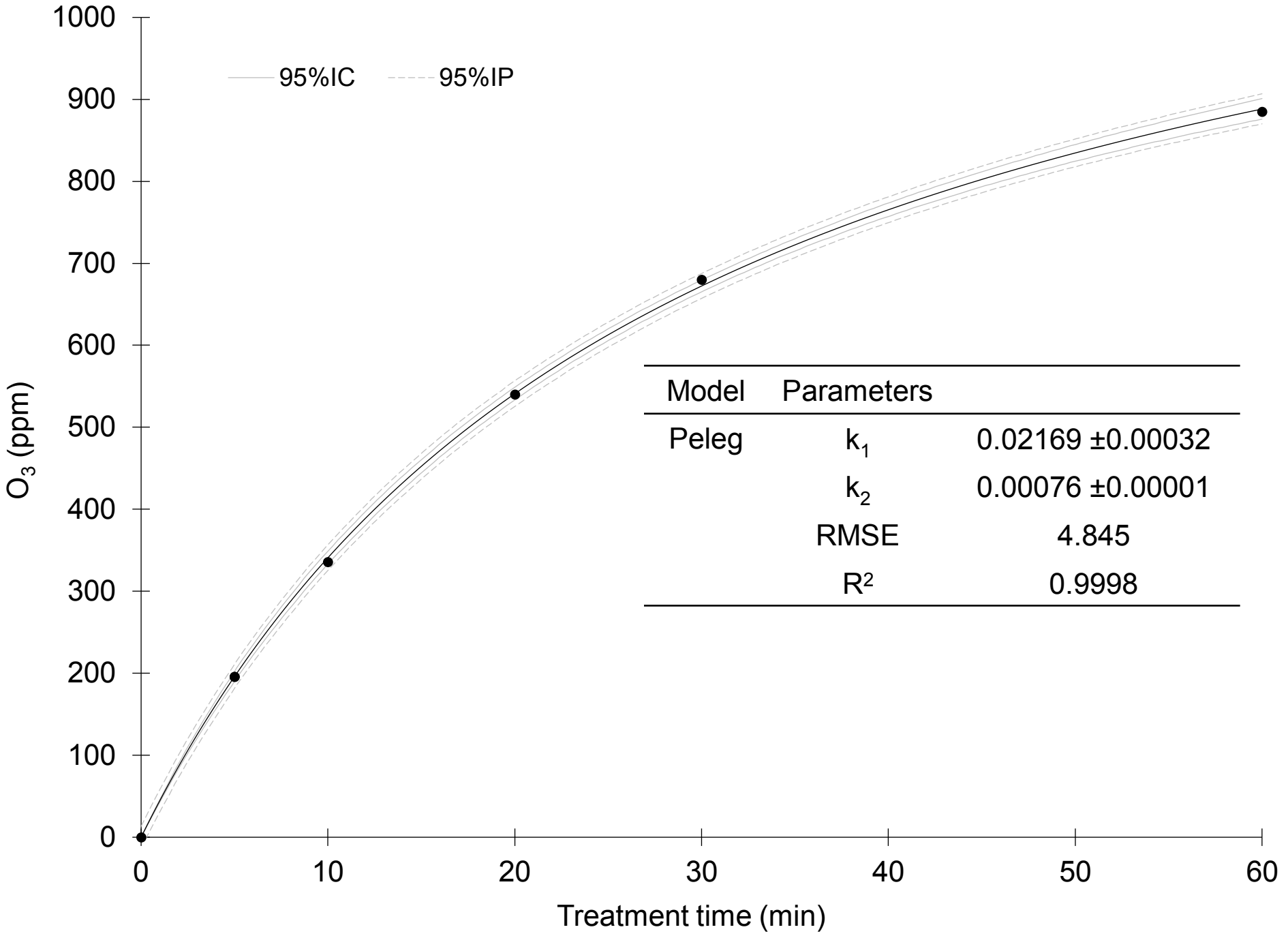

Model	Parameters	
Peleg	k_1	0.02169 ±0.00032
	k_2	0.00076 ±0.00001
	RMSE	4.845
	R^2	0.9998

Figure 2

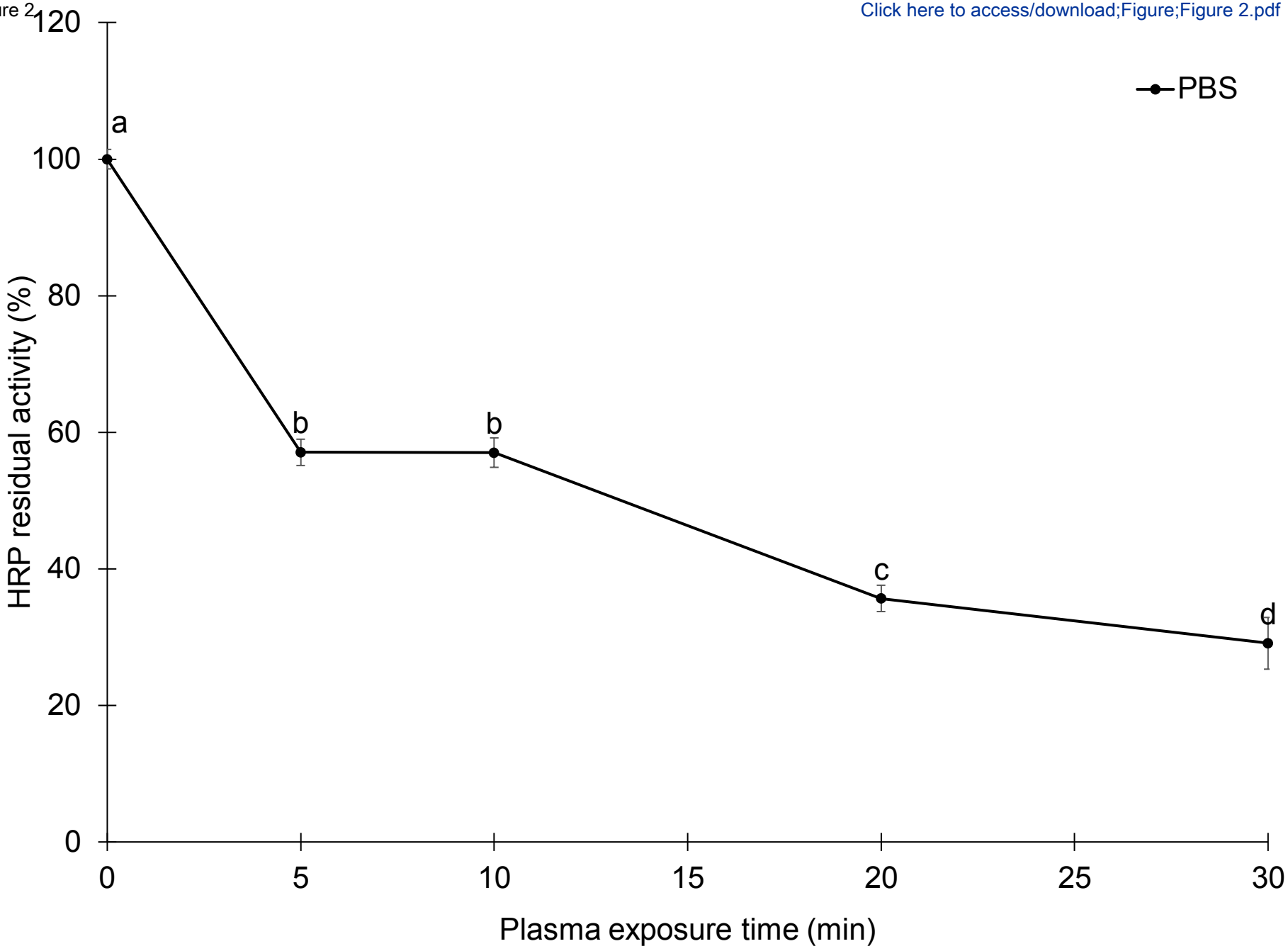

Figure 3

Click here to access/download;Figure;Figure 3.pdf

a)

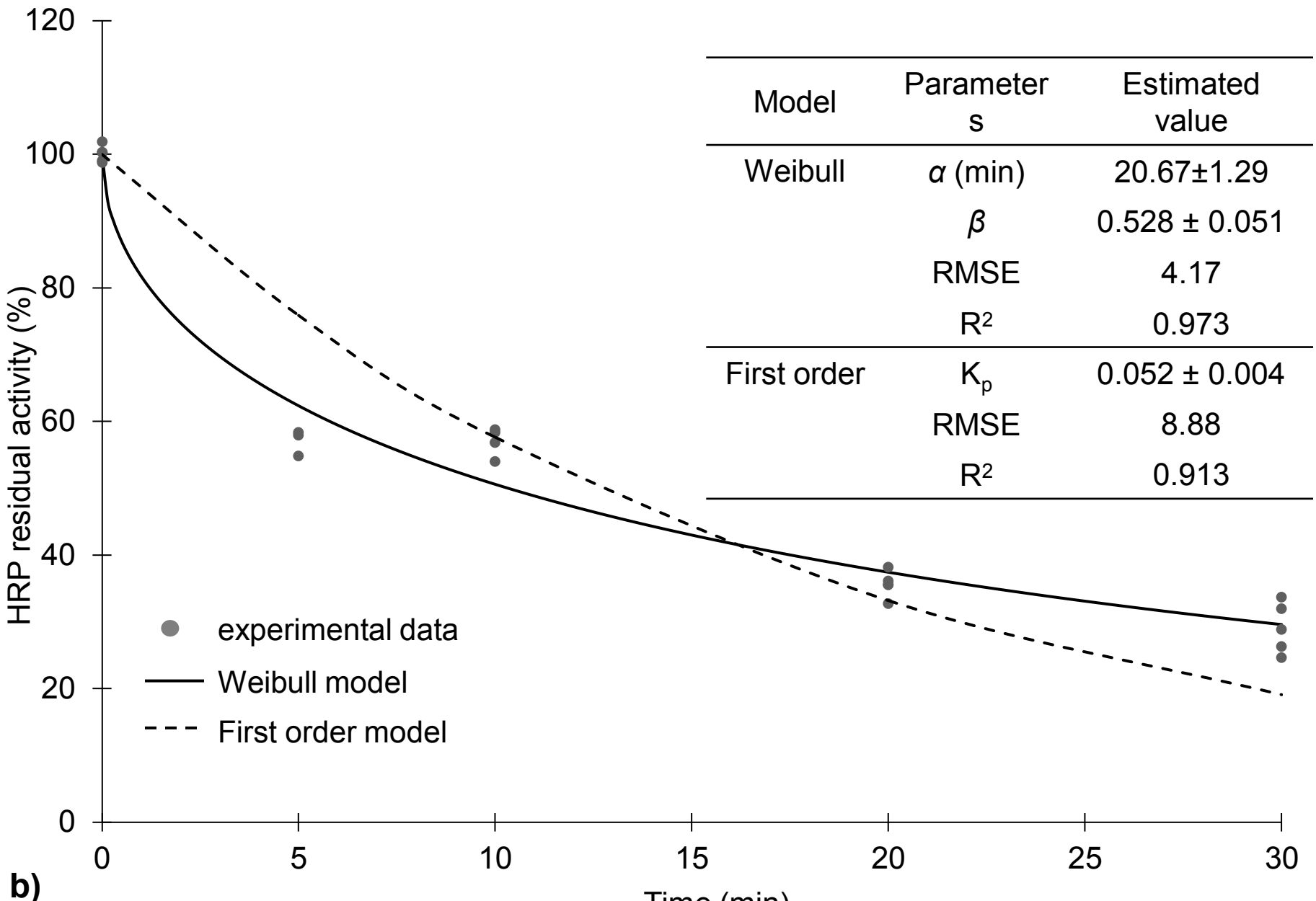

Model	Parameters	Estimated value
Weibull	α (min)	20.67±1.29
	β	0.528 ± 0.051
	RMSE	4.17
	R^2	0.973
First order	K_p	0.052 ± 0.004
	RMSE	8.88
	R^2	0.913

b)

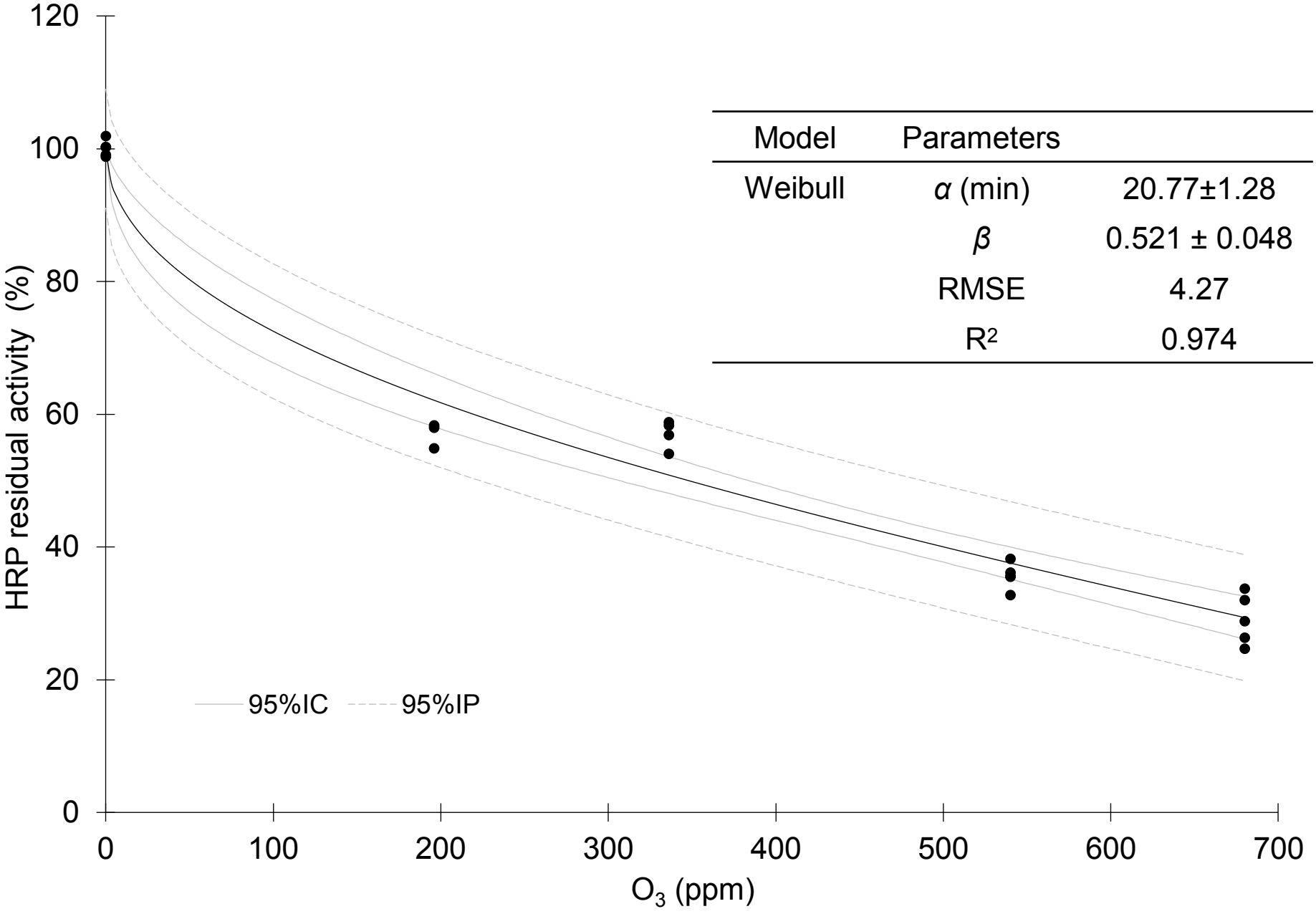

Model	Parameters	
Weibull	α (min)	20.77±1.28
	β	0.521 ± 0.048
	RMSE	4.27
	R^2	0.974

Figure 4

Click here to access/download;Figure;Figure 4.pdf

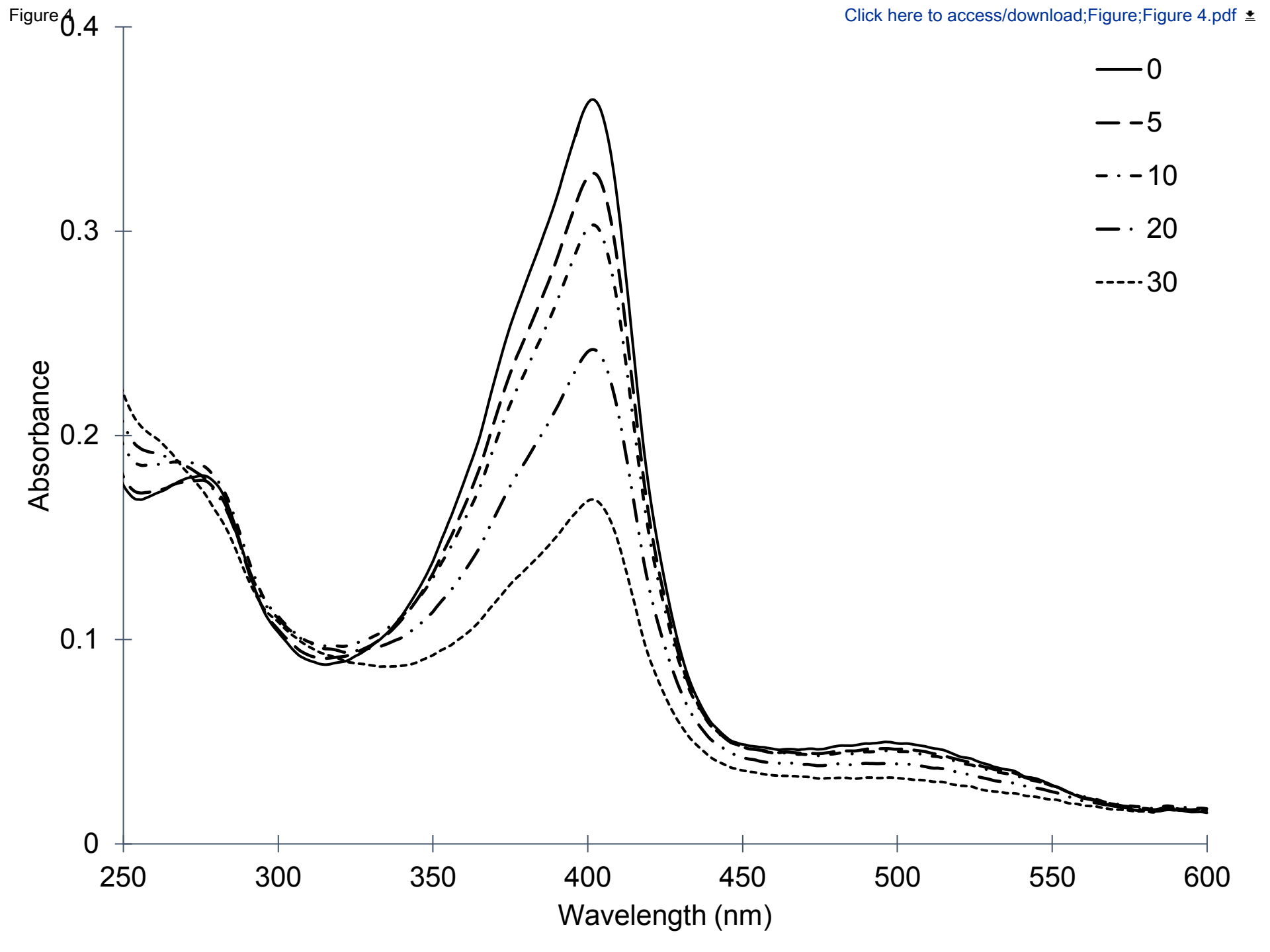

Figure 5

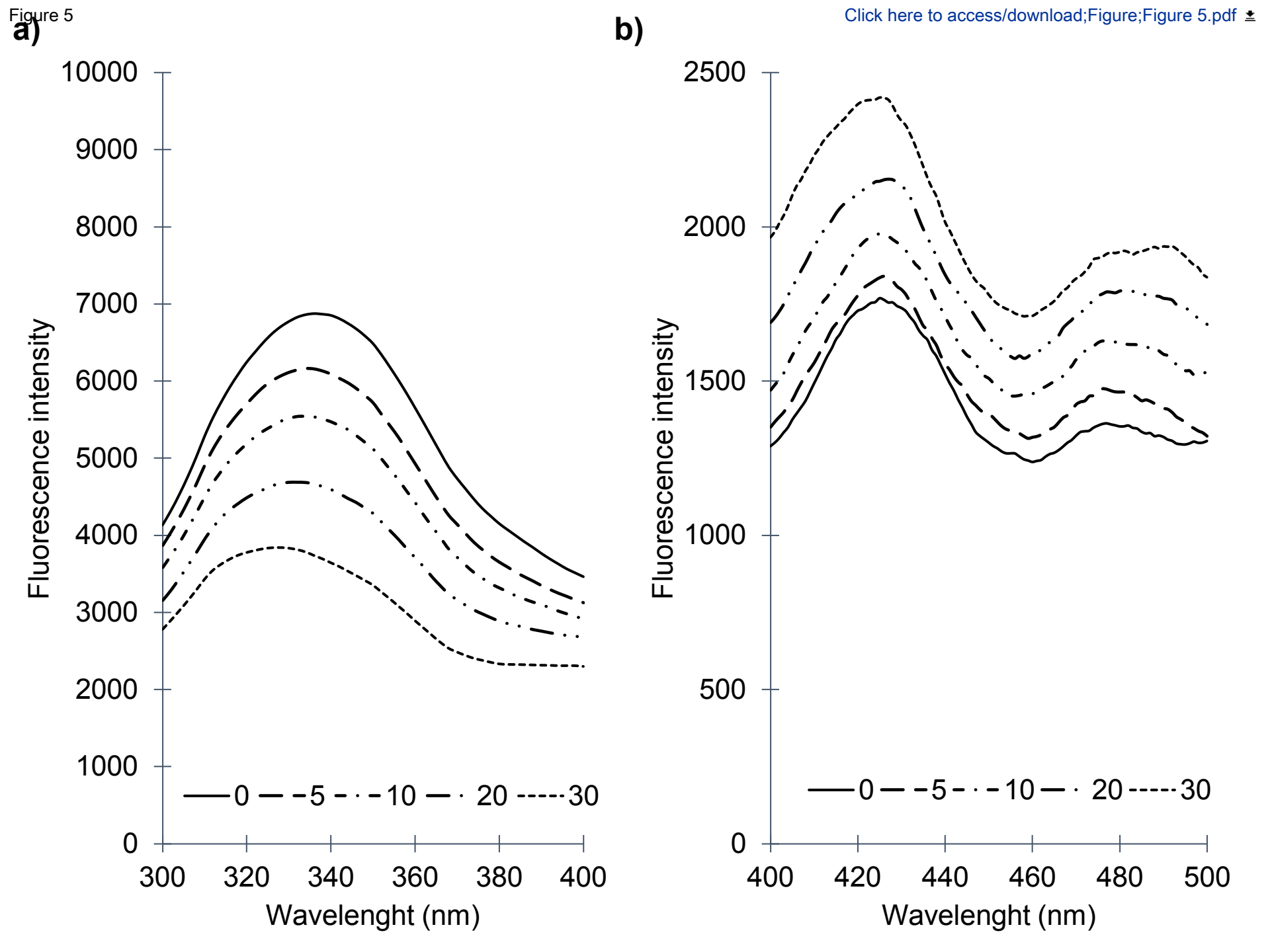

Figure 6

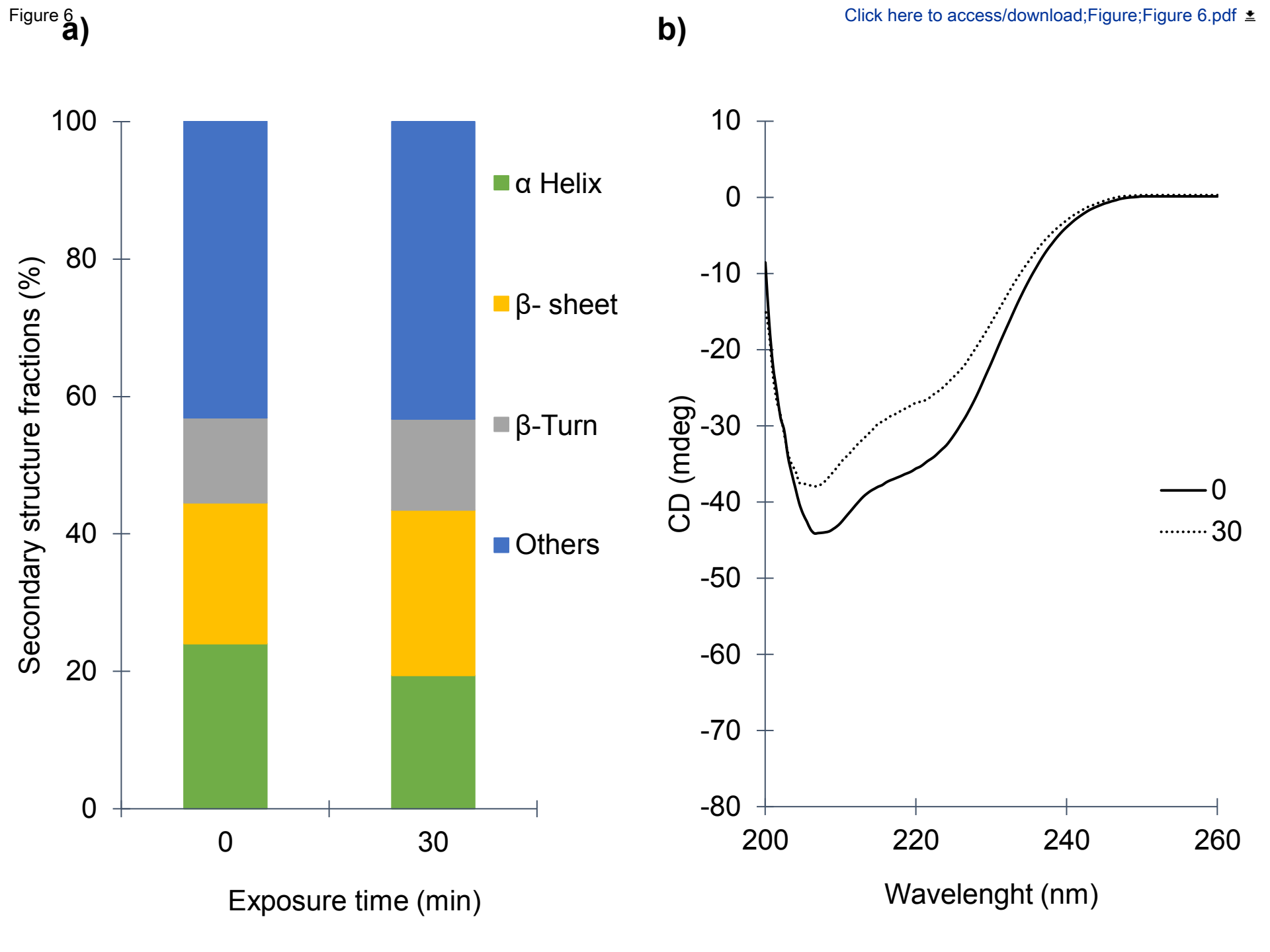

Figure 7

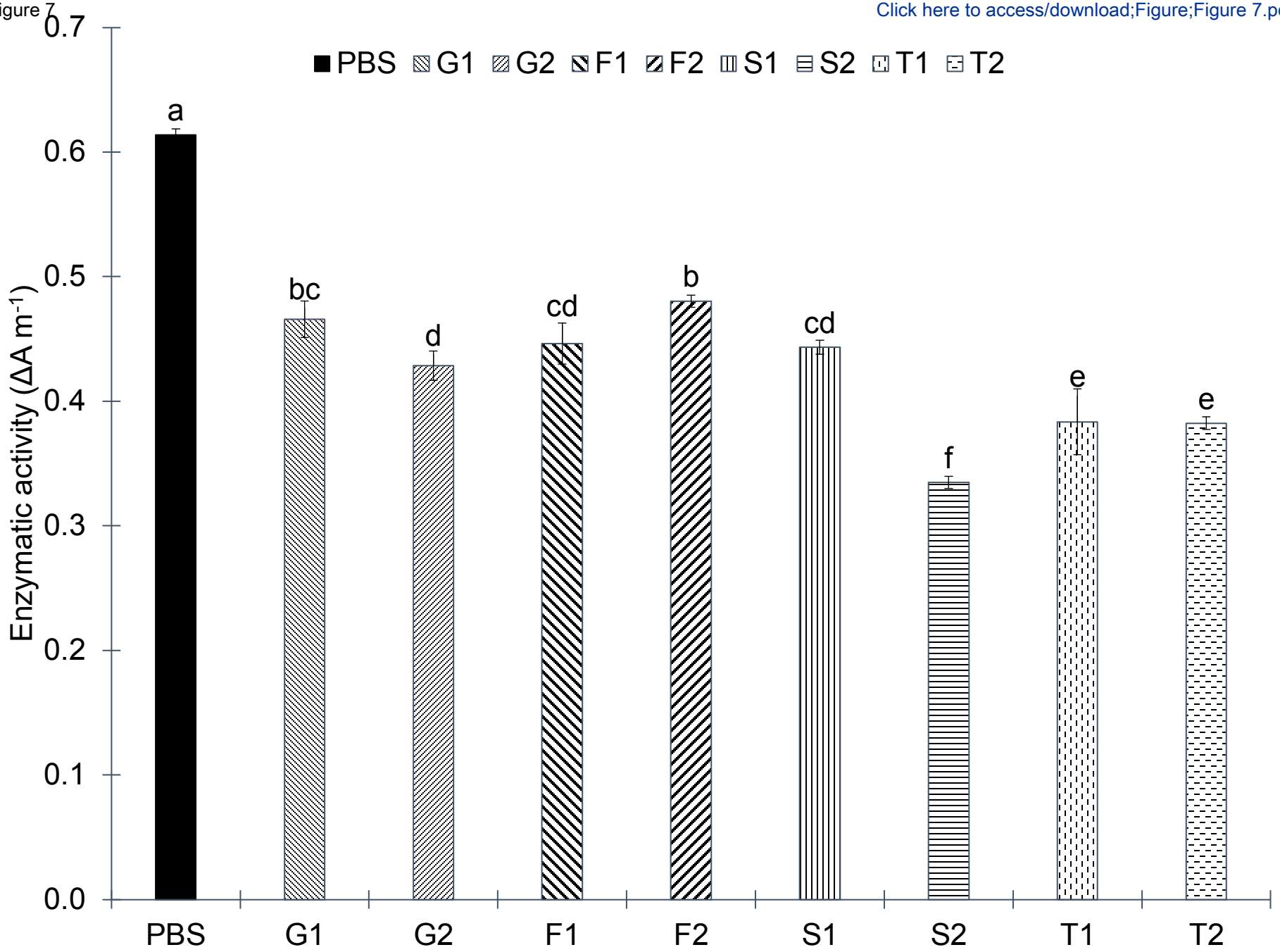

Figure 8

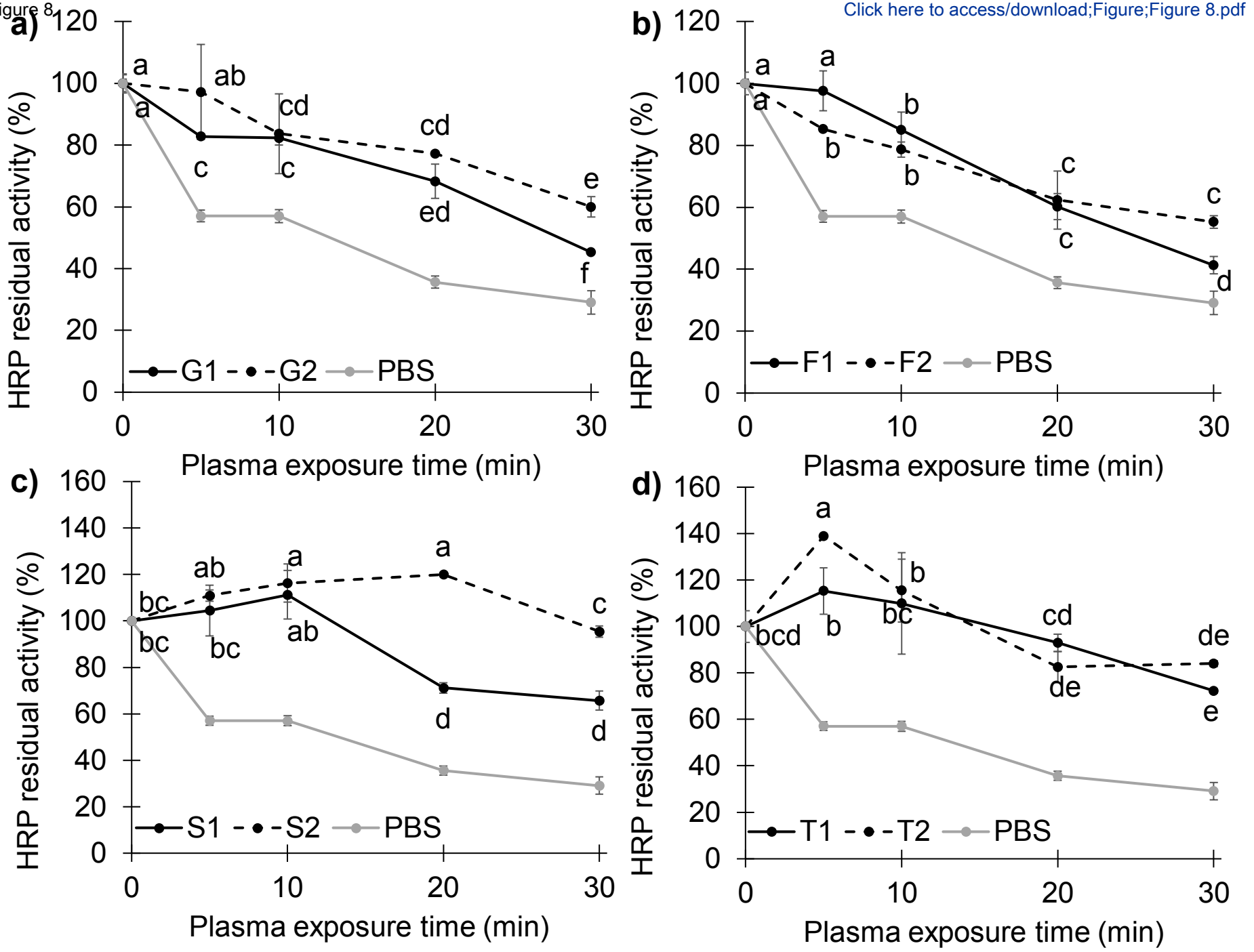

Figure 9

Click here to access/download;Figure;Figure 9.pdf

Figure 10

Click here to access/download;Figure;Figure 10.pdf

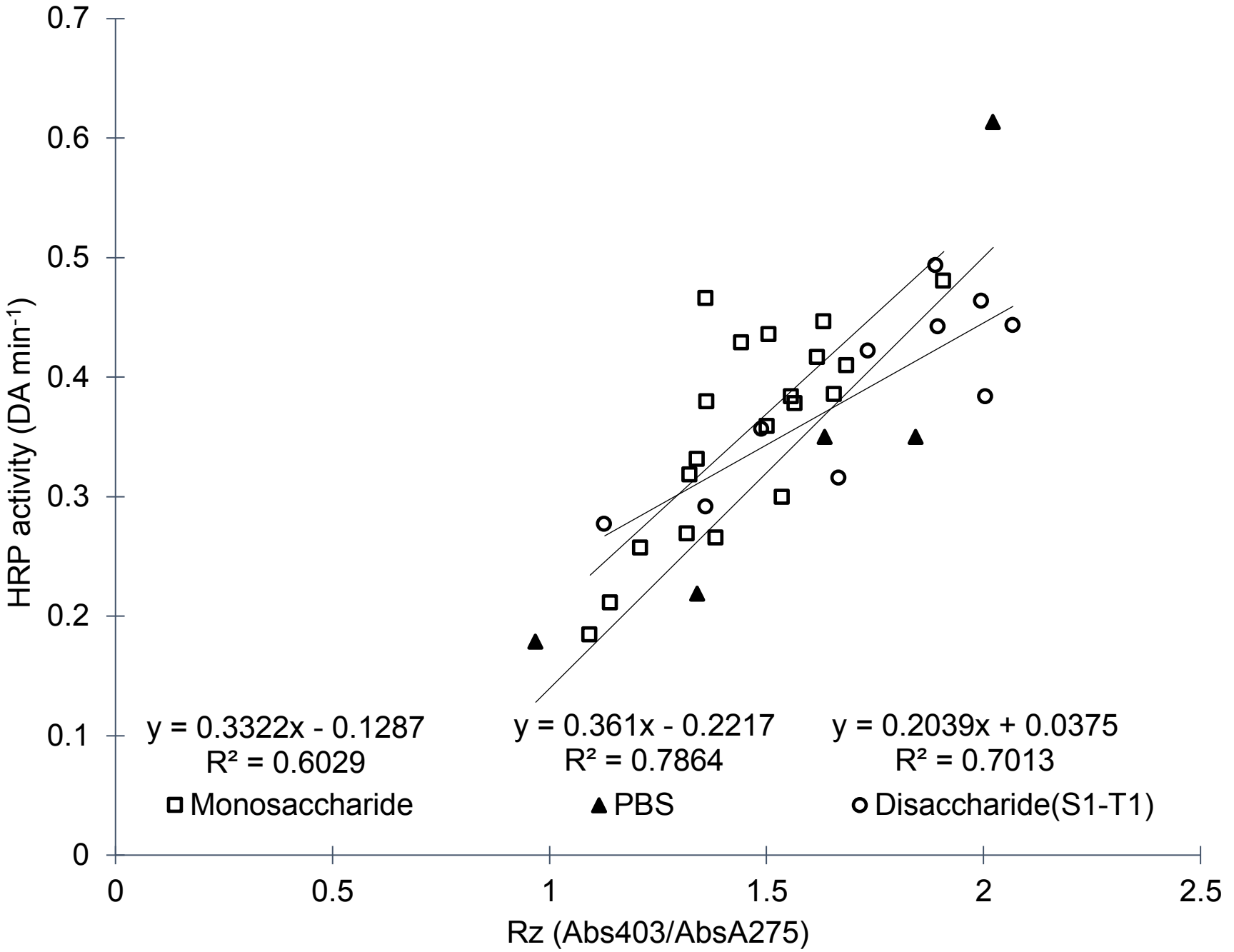

Figure 11

Click here to access/download;Figure;Figure 11.pdf

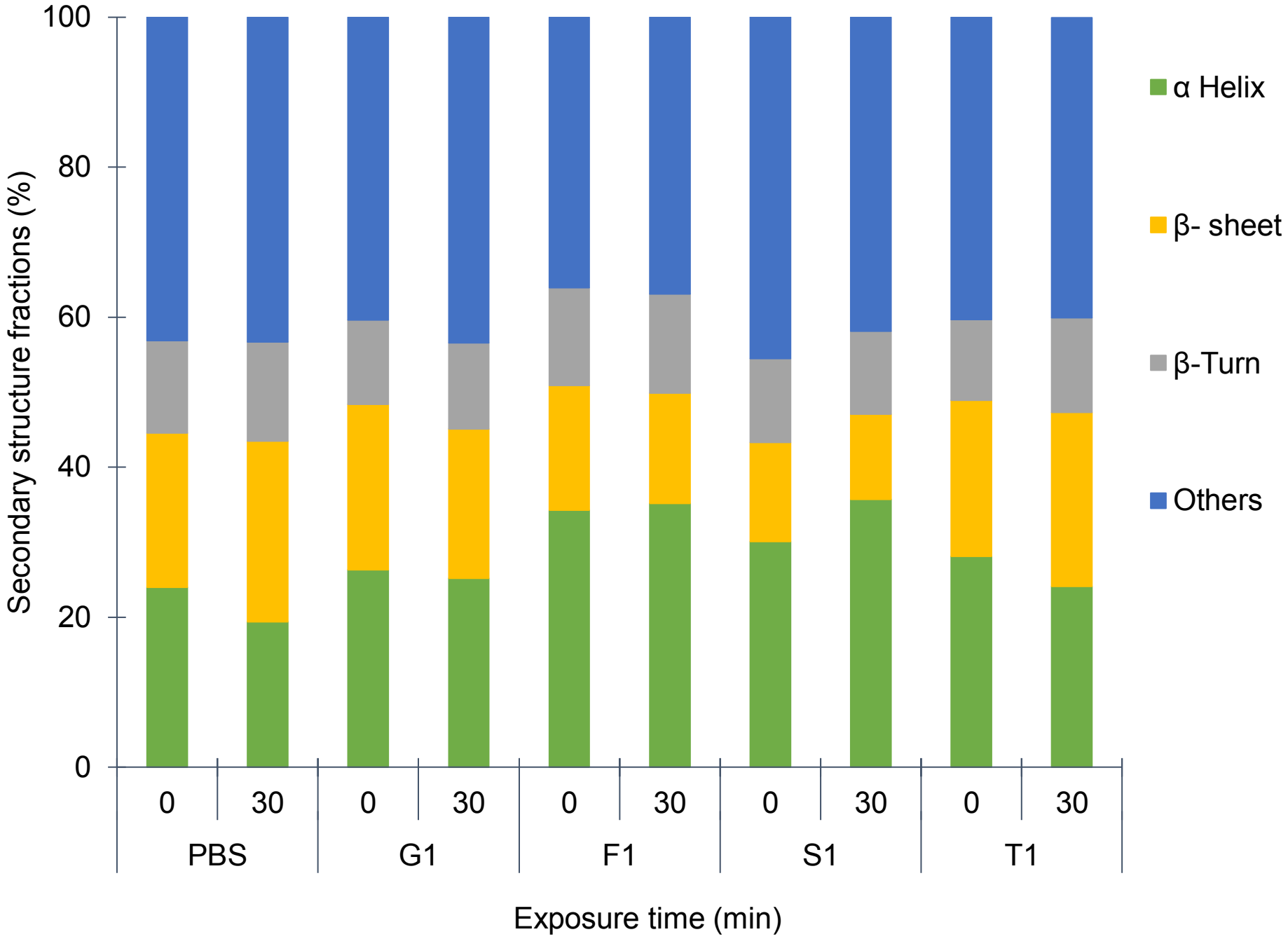

Table 1. Fluorescence emission intensity (I_{max}) and wavelength at maximum emission (λ_{max}) of tryptophan in PBS and sugar model systems before and after different CAP exposures (upper table). For each system, I_{max} and λ_{max} variations (Δ) after CAP treatments were reported (bottom table).

	CAP exposure time (min)					CAP exposure time (min)				
	0	5	10	20	30	0	5	10	20	30
Model system	I_{max}					λ_{max} (nm)				
PBS	6875	6160	5543	4685	3838	336	334	334	332	328
G1	5855	5308	5152	5180	4772	336	334	332	330	326
G2	5733	5279	5103	5213	5046	336	334	334	332	328
F1	4855	4253	3883	3850	3605	336	334	332	330	328
F2	4416	3812	3720	3594	3235	336	336	334	332	328
S1	8577	7176	6545	5704	4675	342	340	340	336	330
S2	9434	7884	7297	6427	5221	348	346	344	342	334
T1	6381	5651	5287	4727	3955	336	334	332	332	326
T2	6873	5562	5437	4892	4274	338	336	334	332	330
	ΔI_{max} (%)					$\Delta\lambda_{max}$ (nm)				
PBS	-	-10.40	-19.38	-31.86	-44.17	-	-2	-2	-4	-8
G1	-	-9.34	-12.00	-11.52	-18.49	-	-2	-4	-6	-10
G2	-	-7.93	-10.99	-9.07	-11.99	-	-2	-2	-4	-8
F1	-	-12.41	-20.01	-20.71	-25.75	-	-2	-4	-6	-8
F2	-	-13.68	-15.76	-18.62	-26.74	-	0	-2	-4	-8
S1	-	-16.34	-23.69	-33.50	-45.50	-	-2	-2	-6	-12
S2	-	-16.43	-22.65	-31.87	-44.66	-	-2	-4	-6	-14
T1	-	-11.43	-17.14	-25.92	-38.02	-	-2	-4	-4	-10
T2	-	-19.07	-20.89	-28.83	-37.82	-	0	-2	-4	-6

The standard error of the analysis was below 2% for all the samples.

Table 2. Pearson correlation coefficient (r) and slope obtained by linear regression of HRP activity ($\Delta A\ min^{-1}$) *vs* I_{max} data collected in monosaccharide (G1, G2, F1, F2) and disaccharide (S1, T1) systems treated by different CAP treatments (0, 5, 10, 20, and 30 min).

Model system	Pearson correlation (r)	Slope
PBS	0.923	0.000131
G1	0.925	0.000224
G2	0.757	0.000193
F1	0.823	0.000192
F2	0.951	0.000191
S1	0.744	0.000046
T1	0.737	0.000052